An RNA-binding protein secreted by *Listeria monocytogenes* activates RIG-I signaling

Alessandro Pagliuso[1,2,3,*], To Nam Tham[1,2,3†], Eric Allemand[4†], Stevens Robertin[1,2,3†], Bruno Dupuy[5,6], Quentin Bertrand[7], Christophe Bécavin[8], Mikael Koutero[1,2,3], Valérie Najburg[9,10], Marie-Anne Nahori[1,2,3], Fabrizia Stavru[1,2,3], Andréa Dessen[7,11], Christian Muchard[4], Alice Lebreton[12], Anastassia V. Komarova[9,10] and Pascale Cossart[1,2,3,*]

[1]Unité des Interactions Bactéries-Cellules, Institut Pasteur, Paris, France

[2]U604 INSERM, Paris, France

[3]USC2020 INRA, Paris, France

[4]Unité de régulation épigénétique, Institut Pasteur, Paris, France

[5]Laboratoire Pathogenèse des Bacteries Anaerobies, Institut Pasteur, Paris, France

[6]Sorbonne Paris Cité, Université Paris Diderot, Paris, France

[7]Univ. Grenoble-Alpes, CNRS, CEA, Institut de Biologie Structurale (IBS), Bacterial Pathogenesis Group, Grenoble, France

[8]Hub de bioinformatique et biostatistique - Centre de Bioinformatique, Biostatistique et Biologie Intégrative, Unité mixte de Service et Recherche 3756 Institut Pasteur - Centre National de la Recherche Scientifique, Paris F-75015, France

[9]Unité de Génomique Virale et Vaccination, Institut Pasteur, Paris, 75015, France

[10]CNRS UMR-3569, Paris, France

[11]Brazilian Biosciences National Laboratory (LNBio), CNPEM, Campinas, SP, Brazil

[12]Équipe Infection et Devenir de l'ARN, Institut de biologie de l'Ecole normale supérieure (IBENS), Ecole normale supérieure, CNRS, INSERM, PSL Université Paris, 75005 Paris, France; INRA, IBENS, 75005 Paris, France

[†]These authors contributed equally to this work

*Correspondence: alessandro.pagliuso@pasteur.fr; pcossart@pasteur.fr

Summary

Recent studies have reported on the presence of bacterial RNA within or outside extracellular membrane vesicles, possibly as ribonucleoprotein complexes. Proteins that bind and stabilize bacterial RNAs in the extracellular environment have not been reported. Here, we show that the bacterial pathogen *Listeria monocytogenes* secretes a small RNA binding protein that we named Zea. We show that Zea binds and stabilizes a subset of *L. monocytogenes* RNAs causing their accumulation in the extracellular medium. Furthermore, Zea binds RIG-I, the vertebrate non-self-RNA innate immunity sensor and potentiates RIG-I-signaling leading to interferon β production. By performing *in vivo* infection, we finally show that Zea modulates *L. monocytogenes* virulence. Together, this study reveals that bacterial extracellular RNAs and RNA binding proteins can affect the host-pathogen crosstalk.

Keywords: RNA-binding protein, extracellular RNA, phage, *Listeria monocytogenes*, bacterial pathogen, virulence factor, RIG-I, type I interferon

Introduction

Listeria monocytogenes (*L. monocytogenes*) is a facultative intracellular pathogen responsible for listeriosis, a severe foodborne disease with high mortality rate in immunocompromised individuals and elderly people (Swaminathan and Gerner-Smidt, 2007). *L. monocytogenes* produces and secretes virulence factors which play a key role in several steps of the bacterial infection process, e.g. the crossing of the intestinal, the blood-brain and the placental barriers, entry and replication inside non phagocytic cells and evasion from the immune system (Radoshevich and Cossart, 2018).

The genes encoding the best-characterized virulence factors of *L. monocytogenes* are located in a 9-kb locus known as *L. monocytogenes* pathogenicity island I (LIPI-I) (Chakraborty et al., 2000; Vazquez-Boland et al., 2001). These factors include the pore-forming toxin listeriolysin O (LLO) (Hamon et al., 2012; Osborne and Brumell, 2017), the two phospholipases PlcA and PlcB (Marquis et al., 1995), the metalloprotease MpI that mediates the maturation of PlcB (Marquis et al., 1997; Poyart et al., 1993), the actin-polymerizing factor ActA (Kocks et al., 1992) and the nucleomodulin OrfX (Prokop et al., 2017). Since these genes are required for crucial steps of the intracellular life cycle of *L. monocytogenes*, their mutation strongly attenuates virulence.

Genome sequencing of *L. monocytogenes* and of the closely related, non-pathogenic *Listeria innocua* paved the way to the identification of new virulence factors (Glaser et al., 2001). The hypothesis has been that uncharacterized proteins, only present in *L. monocytogenes,* could be involved in virulence. Predicted secreted proteins have focused attention because they could directly interact with host components during infection and subvert cellular functions (David et al., 2018; Glaser et al., 2001; Lebreton et al., 2011; Prokop et al., 2017). Secreted proteins were predicted based on the detection of an N-terminal signal sequence that is recognized by the general secretion pathway (Sec) and promotes protein translocation across the bacterial membrane. This approach led, for example, to the identification of LntA, a *L. monocytogenes* nucleomodulin that translocates into the nucleus of infected cells and herein modifies the host transcription program (Lebreton et al., 2011).

In addition to proteins, *L. monocytogenes* exports small molecules and metabolites that play a role during infection. For instance, cyclic-di-AMP is secreted by cytosolic *L. monocytogenes* and constitutes a main trigger of the type I interferon (IFN) response (Woodward et al., 2010).

Secretion of nucleic acids and in particular of RNA has recently garnered attention as a novel way for bacteria to affect the host cell response [reviewed in (Tsatsaronis et al., 2018)]. The best-characterized pathway through which bacteria can secrete RNA is *via* the production of membrane vesicles (MVs), small vesicles enclosed in a single lipid bilayer (Dauros-Singorenko et al., 2018; Tsatsaronis et al., 2018). MVs range from 20 nm to 1000 nm in diameter and are produced during bacterial growth (Toyofuku et al., 2018). The observation that both Gram-positive (Brown et al., 2015; Tsatsaronis et al., 2018) and Gram-negative bacteria (Blenkiron et al., 2016; Ghosal et al., 2015; Ho et al., 2015; Malabirade et al., 2018; Sjostrom et al., 2015) as well as fungi (Peres da Silva et al., 2015) and protists (Bayer-Santos et al., 2014) are able to secrete RNA *via* MVs has led to hypothesize that RNA secretion might be a mechanism shared by microorganisms to affect host physiology. The RNA content from isolated MVs has been recently characterized for several microbial species (Tsatsaronis et al., 2018). Interestingly, MV RNAs significantly differ from the intracellular RNA pool, suggesting that specific RNAs are selectively sorted inside MVs *via* a still uncharacterized mechanism.

A recent study reported that extracellular RNA can be also found outside MVs (Ghosal et al., 2015). Given the high abundance of ribonucleases in the extracellular environment, the authors proposed that the presence of RNA-binding proteins (RBPs) accounts for the stability of the secreted RNAs. However, attempts to identify secreted RBPs in bacteria have been unsuccessful so far (Tawk et al., 2017).

Two recent studies have shown that *L. monocytogenes* secretes RNA in the extracellular environment (Abdullah et al., 2012; Hagmann et al., 2013). The authors found that *L. monocytogenes* secretes RNA into the cytoplasm of infected cells, which triggers the type I IFN response in a RIG-I dependent

89 manner. However, which RNAs are specifically involved in this response as well as the mechanism
90 controlling RNA secretion and accumulation in the extracellular medium remain unaddressed
91 questions.

92 In this study, we provide an in-depth characterization of the first bacterial secreted RBP, the *L.*
93 *monocytogenes* protein Lmo2686. We found that (i) Lmo2686 is secreted; (ii) Lmo2686 is a *bona*
94 *fide* RBP; (iii) Lmo2686 induces extracellular accumulation of a subset of *L. monocytogenes* RNAs
95 possibly by protecting them from degradation; (iv) Lmo2686 modulates *L. monocytogenes* virulence;
96 (v) Lmo2686 interacts with RIG-I and potentiates the RIG-I-dependent IFN response during
97 infection.

98 Based on these findings, we propose to rename this protein Zea, as Zea, also known as Hecate, is an
99 ancient Greek goddess who protected and guided the travelers.

Results

Zea is a small secreted protein of *L. monocytogenes*

The lmo2686/zea open reading frame is 534-bp long and is located 164 bp downstream from the *lmo2687* gene, which encodes an FtsW-related protein. *zea* is followed by a transcriptional terminator upstream from the divergently transcribed *lmo2685* gene, which encodes a cellobiose phosphotransferase protein (**Figure 1A**). *zea* is found in about half of the *L. monocytogenes* strains sequenced to date as well as in the animal pathogen *Listeria ivanovii* (Becavin et al., 2017). Orthologs of *zea* are also found in other species, mainly Gram-positive bacteria of the genus *Bacillus* (**Figure S1**). Interestingly, *zea* is absent from the genome of the nonpathogenic species *L. innocua* (Glaser et al., 2001) and *Listeria marthii* FSL S4-120 (Graves et al., 2010) which suggests that it may play a role in *L. monocytogenes* virulence (**Figure 1A**).

RNA sequencing (RNA-Seq) data has revealed the presence of a transcriptional start site upstream of the start codon of *zea* which indicates that the gene can be transcribed from its own promoter (**Figure 1A**) (Wurtzel et al., 2012). *zea* appears constitutively expressed at 37 ˚C, albeit at low levels, and is slightly more expressed at 30 ˚C and under microaerophilic conditions (Becavin et al., 2017; Wurtzel et al., 2012).

The *zea* gene encodes a small protein of 177 amino acids (aa) (**Figure 1B**). Analysis of the Zea protein sequence predicted the presence of a N-terminal signal peptide of 25 aa for SecA-mediated secretion, resulting in a putative 152 aa mature protein with a basic isoelectric point (pI = 8.4) (**Figure 1B**). We could not identify any other domain or sequence of known function.

The presence of a signal peptide prompted us to test whether Zea could be secreted. We generated three different antibodies against three peptides of the C-terminus of the protein and used them to assess the presence of Zea in the *L. monocytogenes* cytosol and in culture medium. Western blotting analysis revealed that Zea could be recovered from the culture medium, indicating secretion of the protein (**Figure 1C**). Culture medium collected from the *zea*-deleted strain (*Δzea*) did not show any

125 immunoreactive band, thus confirming the specificity of our antibodies. The secretion of Zea was
126 also confirmed by engineering a *L. monocytogenes* strain carrying a chromosome-integrated copy of
127 the C-terminally Flag-tagged *zea* gene under the control of a constitutive promoter (zea^{Flag}-*pAD*)
128 (**Figure 1D**). Quantitative analysis of the repartition of Zea between bacterial cytosol and culture
129 medium in stationary phase revealed a strong accumulation in the extracellular medium indicating
130 that the protein was efficiently secreted (**Figure 1D**).

131

132 **Zea is an oligomeric protein that interacts with RNA**

133 The structure of Zea was previously solved by X-ray crystallography at a resolution of 2.75 Å and
134 deposited in the Protein Data Bank (PDB) by Minasov G. and colleagues (PDB ID: 4K15;
135 https://www.ebi.ac.uk/pdbe/entry/pdb/4K15). According to this structure, Zea is a toroid-shaped
136 homohexamer in which every monomer contacts the neighboring one *via* a beta-hairpin-beta unit
137 (**Figure 2A**). As this structure is not shared by any other polypeptide of known function, at present,
138 the role of Zea and of its orthologs in other species is unknown.

139 We noticed that several other proteins that assemble as a torus, like Zea, have the intrinsic capability
140 to bind RNA (Antson et al., 1995; Babitzke et al., 1995; Lee et al., 2007; Thomsen and Berger, 2009;
141 Vogel and Luisi, 2011). Interestingly, Zea shows a positively charged surface on one side of the torus,
142 due to the presence of several lysine residues, which might well accommodate the negatively-charged
143 RNA (**Figure 2B**). These features led us to hypothesize that Zea might bind RNA.

144 Before addressing this hypothesis, we sought to verify whether the oligomeric state of Zea observed
145 by X-ray crystallography also existed under physiological conditions, ruling out possible
146 crystallization artifacts. We used three different approaches: (i) co-immunoprecipitation of HA- and
147 Flag-tagged versions of Zea (**Figure 2C**), (ii) size exclusion chromatography of *L. monocytogenes*
148 cytosol and culture medium (**Figure 2D**) and (iii) size exclusion gel chromatography of recombinant
149 His-tagged Zea expressed and purified from *E. coli* (**Figure 2E**). Collectively, our data show that Zea

has a high tendency to oligomerize, in line with its hexameric structure shown by X-ray crystallography.

We then examined whether Zea could bind RNA. We performed RNA immunoprecipitation (IP) followed by high-throughput sequencing (RIP-Seq) by using the protocol schematized in **Figure S2**. Given the low amount of Zea protein produced *in vitro*, we made use of a Zea-overexpressing strain (*zea-pAD*). Zea was immunoprecipitated from *L. monocytogenes* cytosol and culture medium and the Zea-bound RNAs were subsequently extracted and sequenced. As a control, we performed a mock IP, using an unrelated antibody of the same isotype. Remarkably, RIP-Seq analysis revealed the presence of several *L. monocytogenes* RNAs, which were highly enriched compared to the control samples (**Figure 2F**), indicating that Zea can form complexes with RNA. An enrichment of $\log_2$ fold change ($\log_2$FC) >1.5 (corresponding to an almost three-fold increase) was used as an enrichment threshold for the identification of Zea-associated RNAs. This filtering led to the identification of 18 and 292 RNAs bound to intracellular and secreted Zea, respectively (**Figure 2F**). The enrichment of Zea-bound RNAs was particularly striking in the culture medium fraction with almost 30% of the identified RNAs showing a $\log_2$FC ranging from 2.5 up to 6 (five to sixty times more present in the Zea IP compared to the control IP). Importantly, enrichment of specific RNAs in the Zea IP was uncorrelated to their expression levels (**Figure 2G**), according to the results deposited in Listeriomics, an open access database which integrates all the *L. monocytogenes* transcriptomic data published until 2017 (Becavin et al., 2017). Together, our data suggest that Zea binds specific RNA targets. Indeed, we could not detect binding of the most highly expressed – and most stable – RNAs, such as rRNAs and tRNAs. In contrast, we found that Zea bound preferentially a subset of protein-coding mRNAs and to lesser extent small regulatory RNAs (**Table S1**).

We then analyzed the genomic distribution of Zea-bound RNAs on the *L. monocytogenes* chromosome (**Figure 3A**). It was striking that there was one region particularly over-represented. This locus contains the prophage A118 (**Figure 3A-C**), and the phage RNA was present both in the

bacterial cytosol and in the culture medium (**Table S1**). Cluster of Orthologous Genes (COG) classification highlighted the phage A118 RNA as the most enriched class of Zea-bound RNAs (**Figure S3**). The phage A118 is a temperate phage belonging to the *Syphoviridae* family of double-stranded DNA bacterial viruses (Dorscht et al., 2009).

To validate the interaction of phage A118 RNA with Zea found by RIP-Seq (**Figure 3A-C**), we performed RNA IP coupled to quantitative PCR (RIP-qPCR) analysis. RIP-qPCR confirmed a strong association of Zea to phage RNA, while we could not find any binding to control transcripts that were not enriched in our RIP-Seq dataset (**Figure 3D)**. In agreement with the RIP-Seq data, the enrichment of phage RNA in the culture medium fraction was particularly strong (up to approximately 30 times more compared to control IgG IP) indicating that the phage RNA accumulates extracellularly together with Zea (**Figure 3D)**.

Taken together, our data revealed that Zea is an oligomeric protein that binds a subset of *L. monocytogenes* RNAs both in the bacterial cytosol and in the culture medium.

Zea directly binds *L. monocytogenes* RNA

We next investigated whether Zea could directly bind RNA. We first performed electrophoretic mobility gel shift assay (EMSA) by using recombinant His-tagged Zea (HisZea) and *in vitro*-transcribed radiolabeled RNA. We selected *rli143* and *rli92*, two small RNAs that showed a significant enrichment in the RIP-Seq dataset (eight- and almost three- fold enrichment compared to control IgG IP, respectively; see **Figure 3A**). Incubation of *rli143* or *rli92* with HisZea produced several major shifts, which are likely due to the binding of different Zea oligomers to RNA (**Figure 4A-B**). Importantly, the binding of Zea with both *rli143* and *rli92* was specific, as it was displaced by the addition of increasing amounts of each unlabeled small RNA (**Figure 4C-D**).

To further prove direct binding of Zea with its target RNAs, we performed an RNA pull-down assay, using *in vitro*-transcribed biotinylated RNA and recombinant HisZea. Here, in addition to *rli143* and

rli92, we tested two other small RNAs (*rli18* and *rli1*), which also displayed specific binding to Zea in the RIP-Seq dataset (**Figure 3A**). As a control we employed a small RNA (*rli80*), that was not specifically bound by Zea. Biotinylated small RNAs were incubated with HisZea and then recovered by streptavidin-coupled beads. After extensive washing, the amount of bound HisZea was assessed by western blotting. Using this approach, we detected binding above background level for three of the four small RNAs tested (**Figure 4E**). Importantly, *rli143*, which showed the highest enrichment in the RIP-Seq dataset, was also the strongest binder of Zea in both the gel shift assay and the pull-down experiments, further validating the RIP-Seq results.

Collectively, these data clearly indicate that Zea can stably and directly bind RNA.

Extracellular Zea-bound RNAs do not derive from bacterial lysis

It was of interest to assess that the extracellular RNAs in complex with Zea were not due to bacterial lysis. We thus first analyzed the presence of one of the most abundant cytosolic proteins of *L. monocytogenes* (EF-Tu) in the culture medium. While EF-Tu was readily detected in the bacterial cytosol, it was undetectable in the culture medium, indicating that bacterial lysis was negligible under our experimental conditions (**Figure 2D**). As bacteria lyse after death, we stained for dead and live bacteria after growth under the conditions used for the RIP-Seq experiment. Confocal microscopy analysis revealed very few dead bacteria (less than 2%), further confirming minimal bacterial lysis (**Figure S4A**). Finally, we designed an experiment in which we used the strict intracellular localization of the RBP Hfq and of its RNA targets as a readout of bacterial lysis. In *L. monocytogenes*, Hfq has been shown to bind three small RNAs, *LhrA*, *LhrB* and *LhrC* (Christiansen et al., 2006). We reasoned that, if bacterial lysis occurred, we should find Hfq complexed to its RNA targets in the medium. To assess this, *L. monocytogenes* was grown under the conditions used for the Zea RIP-Seq experiment and Hfq was then immunoprecipitated from the bacterial cytosol and culture medium by using a specific anti-Hfq antibody (Christiansen et al., 2006). Hfq was recovered from

the bacterial cytosol but was undetectable in the culture medium, indicating minimal bacterial lysis (**Figure S4B**). RNA was extracted from the immunopurified Hfq ribonucleoprotein complexes and used to assess the abundance of the Hfq targets by qPCR. Given the low expression of *LhrB* and *LhrC* in stationary phase (Christiansen et al., 2006), we focused on *LhrA*. *LhrA* was detected in association with intracellular Hfq, but remained undetectable in the culture medium (**Figure S4C**).

Collectively, these results strongly indicate that extracellular RNAs complexed with Zea are not originating from lysed bacteria.

Zea overexpression induces extracellular accumulation of Zea-binding RNAs

Since Zea binds RNA and is secreted, we sought to determine whether it could affect the amount of secreted RNA in the culture medium. Given the strong binding of Zea to phage RNA (**Figure 3A-D** and **S3**), we compared the amount of phage RNA present in the culture medium of *L. monocytogenes wt*, *Δzea* and *zea-pAD*. For this purpose, *L. monocytogenes* was grown in minimal medium (MM), because rich medium (BHI) contains large quantities of contaminating RNAs. qPCR analysis on RNA extracted from the culture medium revealed that the overexpression of Zea increased the amount of secreted phage RNA (**Figure 5A**). Strikingly, the intracellular abundance of the phage genes was comparable in the three *L. monocytogenes* strains under study **(Figure S6A)**, indicating that Zea specifically affects the quantity of secreted RNAs and not their expression level. However, when comparing *wt* and *Δzea* strains, we did not find remarkable changes in the amount of secreted phage RNA. This is probably due to the low expression level of Zea by *wt* bacteria in MM, as revealed by qPCR (**Figure S5**). We next evaluated the abundance of another class of highly enriched RNAs specifically bound to Zea: the lma-monocin RNAs (**Figure S3**). The lma-monocin locus is considered to be a cryptic prophage specific of the *Listeria* genus whose function remains elusive (Gohmann et al., 1990; Lee et al., 2016). Overexpression of Zea increased the amount of the lma-monocin RNAs in the culture medium (**Figure 5B**), mirroring the results obtained for the A118 phage. Also in this

250 case, the intracellular level of lma-monocin RNA was comparable among the three *L. monocytogenes*
251 strains used **(Figure S6B)**.

252 This approach could not be applied to secreted small RNAs detected by RIP-Seq due to their low
253 expression levels. To overcome this problem, we overexpressed *rli143* in *wt*, *Δzea* and *zea-pAD L.*
254 *monocytogenes* and then measured *rli143* abundance in the culture medium. As a control, we
255 generated a fourth strain overexpressing both *rli143* and Lmo2595, another secreted protein of *L.*
256 *monocytogenes* that, like Zea, harbors a canonical signal peptide (Glaser et al., 2001). In line with the
257 above results, *rli143* accumulated in the culture medium when Zea was co-overexpressed (**Figure**
258 **5C**) but not when Lmo2595 was co-overexpressed. The intracellular expression level of *rli143* was
259 comparable in all the strains (**Figure S6C)**.

260 To further establish a role for Zea in the regulation of the extracellular RNA amount, we generated a
261 *L. innocua* strain overexpressing either *rli143* alone, or *rli143* with Zea, and then measured the
262 abundance of *rli143* in the culture medium. As a control, *rli143* was co-expressed with Lmo2595. Of
263 note, Zea and Lmo2595 are *L. monocytogenes* proteins that are also secreted when expressed in *L.*
264 *innocua* (data not shown). We found that co-expression of Zea and *rli143* induced an even greater
265 accumulation of *rli143* in the culture medium compared to *L. monocytogenes* (**Figure 5D**). The intra-
266 bacterial abundance of *rli143* was comparable in all the *L. innocua* strains (**Figure S6D)**. Altogether,
267 these data show that the overexpression of Zea induces accumulation in the culture medium of phage-
268 derived and small RNAs that are Zea-binding RNA species.

269 Zea overexpression could increase the amount of extracellular RNA by promoting its export from
270 bacteria and/or by promoting its stabilization in the culture medium. Interestingly, we found that Zea
271 protected *rli143* from RNase-mediated degradation *in vitro* (**Figure S7**) indicating that the
272 mechanism of RNA stabilization may partially account for the increased amount of extracellular
273 RNA.

As a last approach to definitively establish the impact of Zea on secreted RNA, we performed RNA-Seq analysis on extracellular RNAs prepared from the *wt* and *zea-pAD* strains. We reasoned that, if Zea increases the secretion and/or protection of a specific subset of secreted *L. monocytogenes* RNAs, then its overexpression should increase the overall amount of those RNAs in the medium. We thus purified extracellular RNA from three independent samples (3 from *wt* and 3 from *zea-pAD*) and performed sequencing. Differential gene expression analysis revealed that, besides the overexpressed Zea RNA, 36 endogenous transcripts were significantly more abundant in the medium of the *zea-pAD* strain (**Figure S8A**). The vast majority of these transcripts were mRNAs (78%), while a small percentage represented sRNAs and antisense RNAs (10% and 8%, respectively) (**Figure S8A**). We then examined the correlation between Zea overexpression and the higher amount of secreted RNA; we intersected the differential extracellular abundance dataset with the dataset of the Zea RIP-Seq experiment performed in the culture medium (i.e. the RNAs in complex with Zea). Strikingly, we found that one third (12 RNAs out of 37) of the transcripts enriched in the culture medium when Zea was overexpressed was also associated with Zea in the RIP-Seq dataset (**Figure S8B**). This indicates that a subset of transcripts found in complex with Zea becomes more abundant in the medium following Zea overexpression (exact right rank fisher's test: p-value = 7.18×10^{-5}). Of note, among these 12 enriched secreted RNAs, 8 RNAs proceeded from the A118 phage. RT-qPCR analysis of intrabacterial phage RNA from the *wt* and *zea-pAD* strains revealed similar amounts of the majority of the phage genes tested, indicating that Zea does not affect the expression of phage genes **(Figure S8C)**.

Altogether, our results show that Zea binds a subset of *L. monocytogenes* RNA and its overexpression increases their abundance in the medium, at least in part by promoting their stabilization.

Zea potentiates the type I IFN response in a RIG-I dependent fashion

Three RBPs of the RIG-I-like receptor (RLR) family (RIG-I, MDA5 and LGP2) can sense non-self RNA in the cytoplasm but only RIG-I and MDA5 can trigger the type I IFN signaling cascade (Chow et al., 2018). A recent approach has successfully helped to identify viral RNA sequences bound either to RIG-I, MDA5 or LGP2 during viral infections (Chazal et al., 2018; Sanchez David et al., 2016). This method is based on the affinity purification of stably expressed Strep-tagged RLRs followed by sequencing of their specific viral RNA partners. We thus applied this approach to obtain *L. monocytogenes*-specific RNAs bound to each of the RLRs upon infection with *L. monocytogenes wt*. We infected HEK293 cells stably expressing Strep-tagged RLRs (or Strep-tagged mCherry as a negative control) with *L. monocytogenes wt* and pulled down the Strep-tagged proteins. Co-purified RNA molecules from three independent replicates were sequenced and mapped to the *L. monocytogenes* genome. We found 15 RNAs specifically enriched in the RIG-I pull-down and, strikingly, 9 of them (60%) belonged to the phage A118 locus (**Figure S9**). We did not identify specific RNAs bound to MDA5 and LGP2, in agreement with a previously suggested major role of RIG-I, and a minor role of MDA5, in *L. monocytogenes*-induced IFN response infection (Abdullah et al., 2012; Hagmann et al., 2013). These data indicate that, during infection, *L. monocytogenes* phage RNAs get access to the host cytoplasm, where they specifically bind to RIG-I.

Since Zea is secreted and binds phage RNAs, we investigated whether it could participate in the RIG-I-dependent signaling. We first compared the expression of IFNβ in cells infected with *L. monocytogenes wt versus* cells infected with *zea-pAD*. qPCR analysis revealed that overexpression of Zea increased the amount of IFNβ while IFNγ was undetectable, as expected in non-immune cells (**Figure 6A**). Importantly, Zea overexpression did not increase the expression of the proinflammatory cytokine interleukin 8 (IL8). Thus, Zea can specifically activate a type I IFNβ response. Next, to address whether the increased IFN response was mediated by RIG-I, we repeated the same experiment in RIG-I knocked-down cells. Strikingly, the Zea-induced IFNβ stimulation was strongly

322 impaired after RIG-I silencing (**Figure 6B**). These data clearly indicate that Zea specifically enhances
323 RIG-I-dependent type I IFN response.

324 The finding that Zea activates RIG-I signaling led us to examine whether the two proteins might share
325 the same localization in cells. Attempts to detect endogenous Zea in infected cells by western blot or
326 immunofluorescence were unsuccessful as our antibodies cross-reacted with unknown mammalian
327 proteins. We thus infected cells with *zea*^{Flag}*-pAD L. monocytogenes* and used an anti-Flag antibody
328 for detection. Western blotting analysis on cytosolic and nuclear fractions prepared from infected
329 cells revealed that Zea was present in both host cell compartments (**Figure S10A**) whereas RIG-I is
330 mostly cytosolic (Liu et al., 2018; Sanchez-Aparicio et al., 2017). Transfected Flag-tagged Zea also
331 localized both to the cytoplasm and the nucleus. (**Figure S10B**). Thus, the fraction of Zea present in
332 the cytosol might be compatible with the RIG-I-dependent signaling. We next tested whether Zea and
333 RIG-I co-localized in cells. We found several loci of co-localization between transfected Flag-tagged
334 Zea and endogenous RIG-I, indicating a spatial vicinity of the two proteins (**Figure 6C**). Of note, a
335 negative control Flag-tagged mCherry protein did not co-localize with RIG-I (**Figure 6C**). These
336 results prompted us to directly test whether Zea could interact with RIG-I. We immunopurified Zea
337 from the culture medium of a *zea*^{Flag}*-pAD* strain and used lysates of HEK293 cells stably expressing
338 Strep-tagged RIG-I as a source of RIG-I protein (Sanchez David et al., 2016). Immunopurified Zea
339 efficiently and reproducibly pulled down Strep-tagged RIG-I from cell lysates, indicating specific
340 interaction between the two proteins (**Figure 6D**). Importantly, this interaction appeared partially
341 stabilized by the presence of *L. monocytogenes* RNA, as pre-treatment of immunopurified Zea with
342 RNaseA, reduced Zea/RIG-I binding, without abolishing it (**Figure 6D**). In agreement with a
343 marginal role of RNA in the Zea/RIG-I interaction, Flag-tagged Zea expressed after transfection in
344 mammalian cells (which is therefore not bound to *L. monocytogenes* RNA) was able to interact with
345 co-expressed Strep-tagged RIG-I, independently of RNA presence (**Figure 6E**). Altogether, our
346 results show that Zea interacts with RIG-I and activates RIG-I-dependent type I IFN response.

Since RIG-I activation implies RNA binding, we sought to determine more precisely whether Zea-bound RNAs could trigger an IFN response. We used a reporter cell line stably transfected with a luciferase gene under the control of a promoter sequence containing five IFN-stimulated response elements (ISRE) (Lucas-Hourani et al., 2013). We found that transfection of the *in vitro*-transcribed Zea-interacting small RNAs showed strong immunostimulatory activity, while an mCherry control transcript did not (**Figure 6F**). This suggests that Zea can induce RIG-I activation in infected cells *via* its associated bacterial RNAs. Importantly, expression of Zea protein alone failed to induce any stimulation, indicating that, despite its capability to physically interact with RIG-I, Zea cannot promote RIG-I activation by itself (**Figure 6G**).

We conclude that during infection, Zea interacts with and activates RIG-I and this activation likely depends on Zea-bound RNA.

Zea modulates *L. monocytogenes* virulence

The absence of a Zea ortholog in *L. innocua* (**Figure 1A**) together with the findings presented above, prompted us to assess whether Zea could impact *L. monocytogenes* virulence. Of note, the *Δzea* strain grew as well as the *wt* strain both in broth and in tissue cultured cells (macrophages and epithelial cells; data not shown). We thus examined the properties of the *wt* and *Δzea* strains in a mouse infection model. After intravenous inoculation, the *Δzea* strain showed a significant increase in bacterial load after 48h and 72h in the liver (**Figure 7A**); a similar effect was observed in the spleen 72h post-inoculation (**Figure 7B)**. These results indicate that Zea is an effector that dampens *L. monocytogenes* virulence.

Discussion

In this study, we identified the first bacterial secreted RBP, the *L. monocytogenes* protein Lmo2686, that we named Zea. We showed that Zea was secreted in the culture medium, where it associated with a subset of *L. monocytogenes* RNAs. The most enriched transcripts in complex with Zea were that of the *L. monocytogenes* phage A118 and RNAs encoded by the phage remnant lma-monocin locus. Interestingly, secretion of phage or phage-related RNAs has been previously observed in other bacterial species, even though the relevance of this finding remains elusive (Ghosal et al., 2015).

We found that overexpression of Zea correlates with an increased amount of its RNA ligands in the culture medium, suggesting that Zea promotes RNA stabilization possibly by protecting bound RNAs from RNase-mediated degradation.

A recent work analyzed the RNA binding potential of 1022 effectors secreted by the types III or IV secretion system of Gram-negative symbionts and bacterial pathogens (Tawk et al., 2017). Using an in-house developed bioinformatic pipeline called APRICOT (Sharan et al., 2017), the authors performed a detailed analysis to predict the presence of classical and non-classical RNA-binding motifs from a reference dataset of RNA-protein interaction studies performed in mammalian cells. Only a limited number of putative secreted bacterial RBPs were identified through this approach and, surprisingly, subsequent cross-linking experiments failed to confirm RNA binding of these RBPs. The authors concluded that secreted RNA-binding effectors are scarce in bacteria.

However, we suspect that some RBPs might not have been detected through this approach. Indeed, analysis of the Zea protein sequence by using RBScore, a recently developed software for the prediction of nucleic acid-binding properties of proteins (Miao and Westhof, 2015), revealed that Zea does not possess any recognizable RNA-binding region. Zea therefore lacks conventional RNA-binding motifs and represents an additional protein to be included in the growing list of noncanonical RBPs (Beckmann et al., 2016; Hentze et al., 2018). It is therefore likely that other bacterial secreted proteins lacking canonical RNA-binding motifs exist and account for the stability of the MV-free

bacterial secreted RNA. As the structure of Zea is already available in PDB (ID: 4K15), mutational analysis should shed light on the residues that are involved in RNA binding and will help finding structural homologues in other bacteria.

L. monocytogenes induces the production of type I IFN during infection (Dussurget et al., 2014). The type I IFN response to *L. monocytogenes* is in part mediated by RIG-I-mediated sensing of bacterial triphosphorylated RNA molecules (Abdullah et al., 2012; Hagmann et al., 2013). Since a *L. monocytogenes ΔsecA2* mutant showed impaired IFNβ production, bacterial RNA secretion seemed to partially depend on the auxiliary protein secretion system SecA2 (Abdullah et al., 2012). Here, we showed that Zea stimulates the RIG-I-dependent IFN response during *L. monocytogenes* infection. Since Zea presents a canonical signal peptide which is predicted to be recognized by the essential SecA machinery, it is unlikely that SecA2 plays a role in the Zea-dependent IFN response. An important question resides in the mechanism by which Zea mediates RIG-I activation. We found that Zea interacts with RIG-I, and that both proteins interact with the phage A118 RNAs. Importantly, Zea-bound RNA can stimulate IFN response. We propose that Zea might contribute to RIG-I activation not only by stabilizing *L. monocytogenes* secreted RNAs, but also by binding to RIG-I and presenting *L. monocytogenes* RNAs for recognition by RIG-I. To our knowledge, Zea is the first bacterial protein shown to interact with RIG-I.

The type I IFN response plays a major role in controlling viral infection. In the context of bacterial infection, however, its function is more complex and opposing roles have been described. In the case of *L. monocytogenes* infections, IFNβ production *in vivo* shows a peak at 24 hours post-infection and is associated with a bacterial growth-promoting activity that is detrimental for the host (Carrero et al., 2004; Dussurget et al., 2014; O'Connell et al., 2004; Stockinger et al., 2009). Accordingly, IFNAR$^{-/-}$ mice have a greatly improved ability to control the bacterial challenge (Auerbuch et al., 2004), indicating that *L. monocytogenes* benefits from the IFN-mediated cellular reprogramming.

Our *in vivo* data revealed that Zea dampens *L. monocytogenes* virulence as its deletion resulted in an increased bacteria burden in the organs of infected mice. Strikingly and in agreement with our results, Zea is absent in the hypervirulent strains of *L. monocytogenes* (lineage I), while it is well conserved in the strains from the lineage II, which includes a smaller number of clinical isolates. This indicates that Zea is a factor that, when present, contributes to render *L. monocytogenes* less virulent. Given the complexity of the innate immune response to *L. monocytogenes* infection, it is difficult to establish the precise role of Zea *in vivo*. Our data point toward a role of Zea in the modulation of the IFN response, but we do not exclude that Zea might have additional roles during infection. We found that Zea also localizes to the nucleus of infected cells (**Figure 7C** and **Figure S10**), possibly to affect host nuclear functions. It is conceivable that the phenotype observed *in vivo* is a consequence of these additional features of Zea.

Given the striking ability of Zea to bind RNA, one important question to address in the future is whether Zea could also bind mammalian RNA during *L. monocytogenes* infection.

Notably, Zea orthologs are also present in other bacteria, that normally reside in the environment and are rarely associated to disease. We do not exclude that, in addition to its role in *L. monocytogenes* virulence, Zea might also play a role during the saprophytic life of *L. monocytogenes*. It has been proposed that secreted RNAs might contribute to communication among bacteria, but their exact role is still largely unexplored (Tsatsaronis et al., 2018). Considering that most bacterial species harboring *zea* orthologs are genetically tractable, the elucidation of the role of Zea-interacting RNAs in environmental bacteria appears to be within reach.

In conclusion, this study revealed the existence of an extracellular ribonucleoprotein complex from bacteria and highlights a novel mechanism involved in the complex host cell response to infection.

Acknowledgments

We thank all members of the Cossart laboratory for helpful discussions. We thank Dr Birgitte Kallipolitis for providing the anti-Hfq antibody. We thank Edith Gouin for production of antibodies. We are grateful to R.Y. Sanchez David and R. Viber for technical support. We thank Jost Enninga, Javier Pizarro-Cerda, Mélanie Hamon, Olivier Dussurget, Hélène Bierne and Filipe Carvalho for critical reading of the manuscript and useful advices.

Author contributions

A.P. designed and conducted most experiments, analyzed data and wrote the manuscript with inputs from F.S., A.L. and A.K.; T.N.T. performed cloning, western blotting, RNA purifications and generated several bacterial strains; E.A. performed gel filtration and RIP-qPCRs; S.R. performed qPCRs and pull-downs; B.D. performed initial gel shift experiments; M.K. performed RLR pull-downs and sequencing; Q.B. and A.D. purified HisZea and performed gel filtrations; C.B. performed bioinformatics analysis; V.N. performed RLR pull-downs, transfection experiments and RNA purifications; M.A.N. performed animal experiments; F.S. performed immunofluorescence experiments; C.M. supervised E.A.; A.L. performed qPCRs and provided strong expertise on data analysis; A.K. provided expertise and tools for the RLR part; P.C. proposed the project to A.P., mentored A.P., supervised the project and edited the manuscript.

Declaration of interests: The authors declare no competing interests.

Funding

This work was supported by grants to P.C.: European Research Council (ERC) Advanced Grant BacCellEpi (670823), ANR Investissement d'Avenir Programme (10-LABX-62-IBEID), ERANET-Infect-ERA PROANTILIS (ANR-13-IFEC-0004-02) and the Fondation Le Roch-Les Mousquetaires. Work in A.L.'s team was supported by Inserm ATIP-Avenir and Mairie de Paris (Programme Émergences–Recherche médicale). P.C. is a Senior International Research Scholar of the Howard Hughes Medical Institute.

References

Abdullah, Z., Schlee, M., Roth, S., Mraheil, M.A., Barchet, W., Bottcher, J., Hain, T., Geiger, S., Hayakawa, Y., Fritz, J.H., *et al.* (2012). RIG-I detects infection with live Listeria by sensing secreted bacterial nucleic acids. EMBO J *31*, 4153-4164.

Allemand, E., Myers, M.P., Garcia-Bernardo, J., Harel-Bellan, A., Krainer, A.R., and Muchardt, C. (2016). A Broad Set of Chromatin Factors Influences Splicing. PLoS Genet *12*, e1006318.

Anders, S., Pyl, P.T., and Huber, W. (2015). HTSeq--a Python framework to work with high-throughput sequencing data. Bioinformatics *31*, 166-169.

Antson, A.A., Otridge, J., Brzozowski, A.M., Dodson, E.J., Dodson, G.G., Wilson, K.S., Smith, T.M., Yang, M., Kurecki, T., and Gollnick, P. (1995). The structure of trp RNA-binding attenuation protein. Nature *374*, 693-700.

Archambaud, C., Gouin, E., Pizarro-Cerda, J., Cossart, P., and Dussurget, O. (2005). Translation elongation factor EF-Tu is a target for Stp, a serine-threonine phosphatase involved in virulence of Listeria monocytogenes. Mol Microbiol *56*, 383-396.

Arnaud, M., Chastanet, A., and Debarbouille, M. (2004). New vector for efficient allelic replacement in naturally nontransformable, low-GC-content, gram-positive bacteria. Appl Environ Microbiol *70*, 6887-6891.

Auerbuch, V., Brockstedt, D.G., Meyer-Morse, N., O'Riordan, M., and Portnoy, D.A. (2004). Mice lacking the type I interferon receptor are resistant to Listeria monocytogenes. J Exp Med *200*, 527-533.

Babitzke, P., Bear, D.G., and Yanofsky, C. (1995). TRAP, the trp RNA-binding attenuation protein of Bacillus subtilis, is a toroid-shaped molecule that binds transcripts containing GAG or UAG repeats separated by two nucleotides. Proc Natl Acad Sci U S A *92*, 7916-7920.

Balestrino, D., Hamon, M.A., Dortet, L., Nahori, M.A., Pizarro-Cerda, J., Alignani, D., Dussurget, O., Cossart, P., and Toledo-Arana, A. (2010). Single-cell techniques using chromosomally tagged fluorescent bacteria to study Listeria monocytogenes infection processes. Appl Environ Microbiol *76*, 3625-3636.

Batsche, E., Yaniv, M., and Muchardt, C. (2006). The human SWI/SNF subunit Brm is a regulator of alternative splicing. Nat Struct Mol Biol *13*, 22-29.

Bayer-Santos, E., Lima, F.M., Ruiz, J.C., Almeida, I.C., and da Silveira, J.F. (2014). Characterization of the small RNA content of Trypanosoma cruzi extracellular vesicles. Mol Biochem Parasitol *193*, 71-74.

Becavin, C., Koutero, M., Tchitchek, N., Cerutti, F., Lechat, P., Maillet, N., Hoede, C., Chiapello, H., Gaspin, C., and Cossart, P. (2017). Listeriomics: an Interactive Web Platform for Systems Biology of Listeria. mSystems *2*.

Beckmann, B.M., Castello, A., and Medenbach, J. (2016). The expanding universe of ribonucleoproteins: of novel RNA-binding proteins and unconventional interactions. Pflugers Arch *468*, 1029-1040.

Blenkiron, C., Simonov, D., Muthukaruppan, A., Tsai, P., Dauros, P., Green, S., Hong, J., Print, C.G., Swift, S., and Phillips, A.R. (2016). Uropathogenic Escherichia coli Releases Extracellular Vesicles That Are Associated with RNA. PLoS One *11*, e0160440.

Brown, L., Wolf, J.M., Prados-Rosales, R., and Casadevall, A. (2015). Through the wall: extracellular vesicles in Gram-positive bacteria, mycobacteria and fungi. Nat Rev Microbiol *13*, 620-630.

Carrero, J.A., Calderon, B., and Unanue, E.R. (2004). Type I interferon sensitizes lymphocytes to apoptosis and reduces resistance to Listeria infection. J Exp Med *200*, 535-540.

Chakraborty, T., Hain, T., and Domann, E. (2000). Genome organization and the evolution of the virulence gene locus in Listeria species. Int J Med Microbiol *290*, 167-174.

Chazal, M., Beauclair, G., Gracias, S., Najburg, V., Simon-Loriere, E., Tangy, F., Komarova, A.V., and Jouvenet, N. (2018). RIG-I Recognizes the 5' Region of Dengue and Zika Virus Genomes. Cell Rep *24*, 320-328.

514 Chevalier, C., Geissmann, T., Helfer, A.C., and Romby, P. (2009). Probing mRNA structure and
515 sRNA-mRNA interactions in bacteria using enzymes and lead(II). Methods Mol Biol *540*, 215-232.
516 Chow, K.T., Gale, M., Jr., and Loo, Y.M. (2018). RIG-I and Other RNA Sensors in Antiviral
517 Immunity. Annu Rev Immunol *36*, 667-694.
518 Christiansen, J.K., Nielsen, J.S., Ebersbach, T., Valentin-Hansen, P., Sogaard-Andersen, L., and
519 Kallipolitis, B.H. (2006). Identification of small Hfq-binding RNAs in Listeria monocytogenes. RNA
520 *12*, 1383-1396.
521 Criscuolo, A., and Brisse, S. (2013). AlienTrimmer: a tool to quickly and accurately trim off multiple
522 short contaminant sequences from high-throughput sequencing reads. Genomics *102*, 500-506.
523 Dauros-Singorenko, P., Blenkiron, C., Phillips, A., and Swift, S. (2018). The functional RNA cargo
524 of bacterial membrane vesicles. FEMS Microbiol Lett *365*.
525 David, D.J., Pagliuso, A., Radoshevich, L., Nahori, M.A., and Cossart, P. (2018). Lmo1656 is a
526 secreted virulence factor of Listeria monocytogenes that interacts with the sorting nexin 6-BAR
527 complex. J Biol Chem *293*, 9265-9276.
528 Dorscht, J., Klumpp, J., Bielmann, R., Schmelcher, M., Born, Y., Zimmer, M., Calendar, R., and
529 Loessner, M.J. (2009). Comparative genome analysis of Listeria bacteriophages reveals extensive
530 mosaicism, programmed translational frameshifting, and a novel prophage insertion site. J Bacteriol
531 *191*, 7206-7215.
532 Dussurget, O., Bierne, H., and Cossart, P. (2014). The bacterial pathogen Listeria monocytogenes
533 and the interferon family: type I, type II and type III interferons. Front Cell Infect Microbiol *4*, 50.
534 Ewels, P., Magnusson, M., Lundin, S., and Kaller, M. (2016). MultiQC: summarize analysis results
535 for multiple tools and samples in a single report. Bioinformatics *32*, 3047-3048.
536 Ghosal, A., Upadhyaya, B.B., Fritz, J.V., Heintz-Buschart, A., Desai, M.S., Yusuf, D., Huang, D.,
537 Baumuratov, A., Wang, K., Galas, D.*, et al.* (2015). The extracellular RNA complement of
538 Escherichia coli. Microbiologyopen *4*, 252-266.
539 Glaser, P., Frangeul, L., Buchrieser, C., Rusniok, C., Amend, A., Baquero, F., Berche, P., Bloecker,
540 H., Brandt, P., Chakraborty, T.*, et al.* (2001). Comparative genomics of Listeria species. Science *294*,
541 849-852.
542 Gohmann, S., Leimeister-Wachter, M., Schiltz, E., Goebel, W., and Chakraborty, T. (1990).
543 Characterization of a Listeria monocytogenes-specific protein capable of inducing delayed
544 hypersensitivity in Listeria-immune mice. Mol Microbiol *4*, 1091-1099.
545 Graves, L.M., Helsel, L.O., Steigerwalt, A.G., Morey, R.E., Daneshvar, M.I., Roof, S.E., Orsi, R.H.,
546 Fortes, E.D., Milillo, S.R., den Bakker, H.C.*, et al.* (2010). Listeria marthii sp. nov., isolated from the
547 natural environment, Finger Lakes National Forest. Int J Syst Evol Microbiol *60*, 1280-1288.
548 Hagmann, C.A., Herzner, A.M., Abdullah, Z., Zillinger, T., Jakobs, C., Schuberth, C., Coch, C.,
549 Higgins, P.G., Wisplinghoff, H., Barchet, W.*, et al.* (2013). RIG-I detects triphosphorylated RNA of
550 Listeria monocytogenes during infection in non-immune cells. PLoS One *8*, e62872.
551 Hamon, M.A., Ribet, D., Stavru, F., and Cossart, P. (2012). Listeriolysin O: the Swiss army knife of
552 Listeria. Trends Microbiol *20*, 360-368.
553 Hentze, M.W., Castello, A., Schwarzl, T., and Preiss, T. (2018). A brave new world of RNA-binding
554 proteins. Nat Rev Mol Cell Biol *19*, 327-341.
555 Ho, M.H., Chen, C.H., Goodwin, J.S., Wang, B.Y., and Xie, H. (2015). Functional Advantages of
556 Porphyromonas gingivalis Vesicles. PLoS One *10*, e0123448.
557 Kocks, C., Gouin, E., Tabouret, M., Berche, P., Ohayon, H., and Cossart, P. (1992). L.
558 monocytogenes-induced actin assembly requires the actA gene product, a surface protein. Cell *68*,
559 521-531.
560 Langmead, B., and Salzberg, S.L. (2012). Fast gapped-read alignment with Bowtie 2. Nat Methods
561 *9*, 357-359.
562 Lebreton, A., Lakisic, G., Job, V., Fritsch, L., Tham, T.N., Camejo, A., Mattei, P.J., Regnault, B.,
563 Nahori, M.A., Cabanes, D.*, et al.* (2011). A bacterial protein targets the BAHD1 chromatin complex
564 to stimulate type III interferon response. Science *331*, 1319-1321.

565 Lee, G., Chakraborty, U., Gebhart, D., Govoni, G.R., Zhou, Z.H., and Scholl, D. (2016). F-Type
566 Bacteriocins of Listeria monocytogenes: a New Class of Phage Tail-Like Structures Reveals Broad
567 Parallel Coevolution between Tailed Bacteriophages and High-Molecular-Weight Bacteriocins. J
568 Bacteriol *198*, 2784-2793.
569 Lee, H.H., Kim, H.S., Kang, J.Y., Lee, B.I., Ha, J.Y., Yoon, H.J., Lim, S.O., Jung, G., and Suh, S.W.
570 (2007). Crystal structure of human nucleophosmin-core reveals plasticity of the pentamer-pentamer
571 interface. Proteins *69*, 672-678.
572 Li, H., Handsaker, B., Wysoker, A., Fennell, T., Ruan, J., Homer, N., Marth, G., Abecasis, G., Durbin,
573 R., and Genome Project Data Processing, S. (2009). The Sequence Alignment/Map format and
574 SAMtools. Bioinformatics *25*, 2078-2079.
575 Liao, Y., Smyth, G.K., and Shi, W. (2014). featureCounts: an efficient general purpose program for
576 assigning sequence reads to genomic features. Bioinformatics *30*, 923-930.
577 Liu, G., Lu, Y., Thulasi Raman, S.N., Xu, F., Wu, Q., Li, Z., Brownlie, R., Liu, Q., and Zhou, Y.
578 (2018). Nuclear-resident RIG-I senses viral replication inducing antiviral immunity. Nat Commun *9*,
579 3199.
580 Love, M.I., Huber, W., and Anders, S. (2014). Moderated estimation of fold change and dispersion
581 for RNA-seq data with DESeq2. Genome Biol *15*, 550.
582 Lucas-Hourani, M., Dauzonne, D., Jorda, P., Cousin, G., Lupan, A., Helynck, O., Caignard, G.,
583 Janvier, G., Andre-Leroux, G., Khiar, S.*, et al.* (2013). Inhibition of pyrimidine biosynthesis pathway
584 suppresses viral growth through innate immunity. PLoS Pathog *9*, e1003678.
585 Malabirade, A., Habier, J., Heintz-Buschart, A., May, P., Godet, J., Halder, R., Etheridge, A., Galas,
586 D., Wilmes, P., and Fritz, J.V. (2018). The RNA Complement of Outer Membrane Vesicles From
587 Salmonella enterica Serovar Typhimurium Under Distinct Culture Conditions. Front Microbiol *9*,
588 2015.
589 Marquis, H., Doshi, V., and Portnoy, D.A. (1995). The broad-range phospholipase C and a
590 metalloprotease mediate listeriolysin O-independent escape of Listeria monocytogenes from a
591 primary vacuole in human epithelial cells. Infect Immun *63*, 4531-4534.
592 Marquis, H., Goldfine, H., and Portnoy, D.A. (1997). Proteolytic pathways of activation and
593 degradation of a bacterial phospholipase C during intracellular infection by Listeria monocytogenes.
594 J Cell Biol *137*, 1381-1392.
595 Mellin, J.R., Tiensuu, T., Becavin, C., Gouin, E., Johansson, J., and Cossart, P. (2013). A riboswitch-
596 regulated antisense RNA in Listeria monocytogenes. Proc Natl Acad Sci U S A *110*, 13132-13137.
597 Miao, Z., and Westhof, E. (2015). Prediction of nucleic acid binding probability in proteins: a
598 neighboring residue network based score. Nucleic Acids Res *43*, 5340-5351.
599 O'Connell, R.M., Saha, S.K., Vaidya, S.A., Bruhn, K.W., Miranda, G.A., Zarnegar, B., Perry, A.K.,
600 Nguyen, B.O., Lane, T.F., Taniguchi, T.*, et al.* (2004). Type I interferon production enhances
601 susceptibility to Listeria monocytogenes infection. J Exp Med *200*, 437-445.
602 Osborne, S.E., and Brumell, J.H. (2017). Listeriolysin O: from bazooka to Swiss army knife. Philos
603 Trans R Soc Lond B Biol Sci *372*.
604 Pereira, J.M., Chevalier, C., Chaze, T., Gianetto, Q., Impens, F., Matondo, M., Cossart, P., and
605 Hamon, M.A. (2018). Infection Reveals a Modification of SIRT2 Critical for Chromatin Association.
606 Cell Rep *23*, 1124-1137.
607 Peres da Silva, R., Puccia, R., Rodrigues, M.L., Oliveira, D.L., Joffe, L.S., Cesar, G.V., Nimrichter,
608 L., Goldenberg, S., and Alves, L.R. (2015). Extracellular vesicle-mediated export of fungal RNA. Sci
609 Rep *5*, 7763.
610 Poyart, C., Abachin, E., Razafimanantsoa, I., and Berche, P. (1993). The zinc metalloprotease of
611 Listeria monocytogenes is required for maturation of phosphatidylcholine phospholipase C: direct
612 evidence obtained by gene complementation. Infect Immun *61*, 1576-1580.
613 Prokop, A., Gouin, E., Villiers, V., Nahori, M.A., Vincentelli, R., Duval, M., Cossart, P., and
614 Dussurget, O. (2017). OrfX, a Nucleomodulin Required for Listeria monocytogenes Virulence. MBio
615 *8*.

Radoshevich, L., and Cossart, P. (2018). Listeria monocytogenes: towards a complete picture of its physiology and pathogenesis. Nat Rev Microbiol *16*, 32-46.

Ramirez, F., Ryan, D.P., Gruning, B., Bhardwaj, V., Kilpert, F., Richter, A.S., Heyne, S., Dundar, F., and Manke, T. (2016). deepTools2: a next generation web server for deep-sequencing data analysis. Nucleic Acids Res *44*, W160-165.

Robinson, M.D., McCarthy, D.J., and Smyth, G.K. (2010). edgeR: a Bioconductor package for differential expression analysis of digital gene expression data. Bioinformatics *26*, 139-140.

Sanchez David, R.Y., Combredet, C., Sismeiro, O., Dillies, M.A., Jagla, B., Coppee, J.Y., Mura, M., Guerbois Galla, M., Despres, P., Tangy, F.*, et al.* (2016). Comparative analysis of viral RNA signatures on different RIG-I-like receptors. Elife *5*, e11275.

Sanchez-Aparicio, M.T., Ayllon, J., Leo-Macias, A., Wolff, T., and Garcia-Sastre, A. (2017). Subcellular Localizations of RIG-I, TRIM25, and MAVS Complexes. J Virol *91*.

Sharan, M., Forstner, K.U., Eulalio, A., and Vogel, J. (2017). APRICOT: an integrated computational pipeline for the sequence-based identification and characterization of RNA-binding proteins. Nucleic Acids Res *45*, e96.

Sjostrom, A.E., Sandblad, L., Uhlin, B.E., and Wai, S.N. (2015). Membrane vesicle-mediated release of bacterial RNA. Sci Rep *5*, 15329.

Stockinger, S., Kastner, R., Kernbauer, E., Pilz, A., Westermayer, S., Reutterer, B., Soulat, D., Stengl, G., Vogl, C., Frenz, T.*, et al.* (2009). Characterization of the interferon-producing cell in mice infected with Listeria monocytogenes. PLoS Pathog *5*, e1000355.

Swaminathan, B., and Gerner-Smidt, P. (2007). The epidemiology of human listeriosis. Microbes Infect *9*, 1236-1243.

Tawk, C., Sharan, M., Eulalio, A., and Vogel, J. (2017). A systematic analysis of the RNA-targeting potential of secreted bacterial effector proteins. Sci Rep *7*, 9328.

Thomsen, N.D., and Berger, J.M. (2009). Running in reverse: the structural basis for translocation polarity in hexameric helicases. Cell *139*, 523-534.

Toyofuku, M., Nomura, N., and Eberl, L. (2018). Types and origins of bacterial membrane vesicles. Nat Rev Microbiol.

Trieu-Cuot, P., Carlier, C., Poyart-Salmeron, C., and Courvalin, P. (1991). Shuttle vectors containing a multiple cloning site and a lacZ alpha gene for conjugal transfer of DNA from Escherichia coli to gram-positive bacteria. Gene *102*, 99-104.

Tsatsaronis, J.A., Franch-Arroyo, S., Resch, U., and Charpentier, E. (2018). Extracellular Vesicle RNA: A Universal Mediator of Microbial Communication? Trends Microbiol *26*, 401-410.

Varet, H., Brillet-Gueguen, L., Coppee, J.Y., and Dillies, M.A. (2016). SARTools: A DESeq2- and EdgeR-Based R Pipeline for Comprehensive Differential Analysis of RNA-Seq Data. PLoS One *11*, e0157022.

Vazquez-Boland, J.A., Kuhn, M., Berche, P., Chakraborty, T., Dominguez-Bernal, G., Goebel, W., Gonzalez-Zorn, B., Wehland, J., and Kreft, J. (2001). Listeria pathogenesis and molecular virulence determinants. Clin Microbiol Rev *14*, 584-640.

Vogel, J., and Luisi, B.F. (2011). Hfq and its constellation of RNA. Nat Rev Microbiol *9*, 578-589.

Woodward, J.J., Iavarone, A.T., and Portnoy, D.A. (2010). c-di-AMP secreted by intracellular Listeria monocytogenes activates a host type I interferon response. Science *328*, 1703-1705.

Wu, T.D., Reeder, J., Lawrence, M., Becker, G., and Brauer, M.J. (2016). GMAP and GSNAP for Genomic Sequence Alignment: Enhancements to Speed, Accuracy, and Functionality. Methods Mol Biol *1418*, 283-334.

Wurtzel, O., Sesto, N., Mellin, J.R., Karunker, I., Edelheit, S., Becavin, C., Archambaud, C., Cossart, P., and Sorek, R. (2012). Comparative transcriptomics of pathogenic and non-pathogenic Listeria species. Mol Syst Biol *8*, 583.

Figure 1. Zea is a secreted *L. monocytogenes* protein

(**A**) Syntheny analysis of the *lmo2686*/*zea*-containing genomic locus between *L. monocytogenes* and *L. innocua* showing the absence of the *lmo2686/zea* gene in *L. innocua.* Arrows represent the transcriptional start sites (TSS). The stem and circle represent the transcriptional terminators. (**B**) Schematic representation (top) and primary sequence (bottom) of the Zea protein. The N-terminal signal peptide of 25 amino acids is highlighted in red. (**C**) Bacterial cytosol and culture medium were prepared from *L. monocytogenes wt* and *Δzea* strains and immunoblotted with the indicated antibodies. EF-Tu and InlC were used as markers of the bacterial cytosol and culture medium, respectively. (**D**) Bacterial cytosol and culture medium from *L. monocytogenes wt* and a Flag-tagged Zea-overexpressing *L. monocytogenes* strain (zea^{Flag}-*pAD*) were immunoblotted with the indicated antibodies. Values of the relative abundance of ZeaFlag for one representative western blot were generated with ImageJ.

Figure 2. Zea is an oligomeric protein that interacts with a subset of *L. monocytogenes* RNAs

(**A**) Ribbon diagram of hexameric Zea. Every monomer is depicted with a different color. (**B**) Electrostatic potential surface representation of the Zea hexamer. The molecule is rotated by 90 °C about the *y*-axis in the successive images. (**C**) Immunoprecipitation (IP) of Zea with an anti-Flag antibody from bacterial cytosol and culture medium from a *L. monocytogenes* strain co-overexpressing ZeaFlag and ZeaHA. The starting material (Input) and Flag-immunoprecipitated proteins (IP: αFlag) were probed by western blotting (WB) with an anti-Flag and with an anti-HA antibodies: starting material (Input) and Flag-immunoprecipitated proteins (IP: αFlag). (**D**) ZeaFlag elution from size exclusion gel chromatography. *L. monocytogenes* bacterial cytosol and culture medium were applied to Superose 6 size exclusion gel chromatography column. An aliquot of each fraction was precipitated with acetone and analyzed by WB with the indicated antibodies. The cytosolic protein EF-Tu serves as a control for the absence of intact or lysed bacteria in the culture medium fraction. (**E**) 280 nm (mAU) absorbance monitoring of a gel filtration profile (Superdex 200)

691 of recombinant purified HisZea (green line). The elution profile of protein markers of known
692 molecular weight is indicated with the orange line. HisZea was purified by Ni^{2+}-affinity followed by
693 size exclusion gel chromatography, analyzed by SDS-PAGE and Coomassie blue staining (top left-
694 hand panel). (**F**) Enrichment of Zea-bound RNAs (n) from bacterial cytosol and culture medium. Blue
695 squares and red circles depict individual RNAs. The y-axis shows the enrichment (expressed as
696 log_2FC) of the Zea-interacting RNAs relative to immunoprecipitation with preimmune serum. (**G**)
697 Expression of *L. monocytogenes* RNAs grown in BHI at stationary phase measured by tiling array
698 compared to the enrichment of the Zea-bound RNAs (expressed as log_2FC).
699
700 **Figure 3. Zea interacts with phage RNA**
701 (**A**) Circular genome map of *L. monocytogenes* showing the position of the Zea-interacting RNAs.
702 The first two circles from the inside show the genes encoded on the + (inner track) and – (outer track)
703 strands, respectively. The positions of Zea-interacting small RNAs (rlis) are pointed at outside of the
704 circular map. Dotted lines highlight the positions of the phage A118 in the *L. monocytogenes* genome.
705 (**B**) Examples of normalized read coverage (reads per million), visualized by IGV from Zea and
706 control (IgG) immunoprecipitations (IP) for a selection of phage A118 phage genes. Genes are
707 depicted with blue arrows. Gene names marked in red show no significant enrichment in the Zea IP
708 compared to IgG IP. (**C**) Heat map showing the fold enrichment of phage A118 transcripts in the Zea
709 IP compared to control IP, in the bacterial cytosol and culture medium for the phage A118 (values
710 are expressed as log_2FC). (**D**) RIP-qPCR (n=2) on RNAs isolated from Zea and control (IgG)
711 immunoprecipitations in the bacterial cytosol (top panel) and culture medium (bottom panel). The
712 enrichment of selected phage (*lmo2282* to *lmo2333*) and control genes was calculated after
713 normalization to the corresponding input fractions. Statistical significance (between the IP IgG and
714 IP αZea is determined by two tailed *t*-test, **P*<0.05, ***P*<0.01, ***P<0.001.
715
716 **Figure 4. Zea directly binds RNA**

(**A, B**) Representative electrophoretic mobility gel shift assay (EMSA) with *in vitro*-transcribed 5'-end radiolabeled *rli143* and *rli92* in the presence of increasing concentration of HisZea, as indicated. (**C, D**) HisZea-*rli143* and HisZea-*rli92* complexes were incubated with increasing concentrations of the corresponding cold competitor RNA. (**E**) Representative WB of streptavidin affinity pull-down of *in vitro*-transcribed biotinylated transcripts (500nM) in the presence of HisZea (400nM). Zea input, 100 ng.

Figure 5. Zea controls the abundance of its target RNAs in the culture medium

qRT-PCR analysis (n=2) on RNA extracted from the culture medium of different *L. monocytogenes* strains (as indicated) for: (**A**) selected phage and control genes; (**B**) the lma-monocin locus; (**C**) *rli143* in *L. monocytogenes*; (**D**) *rli143* in *L. innocua.* The relative abundance was calculated after normalization to the *wt* sample. The dashed lines indicate the relative abundance in the *wt* strain. Statistical significance determined by two tailed *t*-test, **P*<0.05, ***P*<0.01, ***P<0.001.

Figure 6. Zea interacts with RIG-I and stimulates a RIG-I dependent IFN response

(A) RT-qPCR analysis (n>3) of *IFNβ*, *IFNγ* and interleukin 8 (*IL8*) expression in response to infection with *wt* and *zea-pAD L. monocytogenes* in LoVo cells infected for 17 hours (MOI 5). The relative expression was calculated after normalization to (i) the actin as a housekeeping gene and (ii) to the *wt* sample. ND, not detected. (**B**) RT-qPCR (n>4) analysis of IFN*β* expression in response to infection with *wt* and *zea-pAD L. monocytogenes* in LoVo cells transfected with control siRNA (ctrl siRNA) or with RIG-I targeting siRNA (RIG-I siRNA) and infected for 17 hours (MOI 5). Statistical significance was determined by two tailed *t*-test, ***P*<0.01, ***P<0.001. (**C**) Representative confocal images of LoVo cells transfected with Flag-tagged Zea (top panel) or Flag-tagged mCherry (bottom panel), fixed and processed for immunofluorescence by using an anti-Flag antibody (red) and an anti-RIG-I antibody (green). The co-localization between Zea and RIG-I was assessed with a line scan (white line) whose fluorescence intensity is plotted in red for ZeaFlag and in green for RIG-I. Top

743 right insets: magnification of the region in which the line scan was performed. Scale bars, 10 μm. (**D**)
744 Left panel: representative Co-IP between Flag-tagged Zea and Strep-tagged RIG-I. Immunopurified
745 ZeaFlag treated with RNase (+ RNaseA, 100 μg/mL) or untreated (-RNaseA) was incubated with a
746 cell lysate from HEK-293 cells stably expressing Strep-tagged RIG-I (Sanchez David et al., 2016).
747 Input and immunoprecipitated materials (IP) were probed with antibodies against Flag-tag, Strep-tag
748 and tubulin (which served as a negative control). Right panel: quantification of the amount of co-
749 immunoprecipitated Strep-tagged RIG-I in presence or absence of RNaseA. (**E**) Representative Co-
750 IP between Flag-tagged Zea and Strep-tagged RIG-I. LoVo cells were co-transfected with the
751 plasmids encoding Flag-tagged Zea and Strep-tagged RIG-I and ZeaFlag was then
752 immunoprecipitated and treated with RNase (+ RNaseA, 100 μg/mL) or untreated (-RNaseA) before
753 elution with an anti-Flag peptide. Input and immunoprecipitated materials (IP) were probed with
754 antibodies against Flag-tag, Strep-tag and tubulin (which served as a negative control). (**F**) The
755 immunostimulatory activity of Zea-interacting small RNAs (*rli143*, *rli18* and *rli92*) was assessed by
756 transfection into ISRE reporter cells lines (Lucas-Hourani et al., 2013) (n=3). Firefly luciferase
757 activity was measured and normalized to mock-transfected cells. *HMW* (high molecular weight),
758 *LMW* (low molecular weight) and *5'3P* (5' triphosphate-RNA) were used as positive controls. An
759 *mCherry* RNA fragment served as a negative control. (**G**) The immunostimulatory activity of the Zea
760 protein was assessed by transfection of a Zea-encoding plasmid (*zea*) into the ISRE reporter cells line
761 (Lucas-Hourani et al., 2013) (n=3). Transfection of an empty plasmid (*empty*) served as a negative
762 control. Firefly luciferase activity was measured and normalized to mock transfected cells. Statistical
763 significance was determined by two tailed *t*-test, **P*<0.05, ***P*<0.01, ***P<0.001.
764
765 **Figure 7. Zea regulates *L. monocytogenes* virulence**
766 Balb/c mice were inoculated intravenously with 1 x 10^4 CFUs of the *L. monocytogenes* EGD-e (*wt*)
767 or the strain deleted of the *zea* gene (*Δzea*) (n=2). After 48 h and 72 h post-infection, livers (**A**) and
768 spleens (**B**) were recovered and CFUs per organ were assessed by serial dilution and plating. The

769 number of bacteria in each organ is expressed as $\log_{10}$ CFUs. Black circles and squares depict

770 individual animals. The lines denote the average ±SEM. *P<0.05; **P<0.01 (two tailed t-tests).

CONTACT FOR REAGENT AND RESOURCE SHARING

Further information and requests for resources and reagents should be directed to and will be fulfilled by the lead contacts Pascale Cossart (pcossart@pasteur.fr) and Alessandro Pagliuso (alessandro.pagliuso@pasteur.fr).

EXPERIMENTAL MODEL AND SUBJECT DETAILS

Bacterial strains and cell lines

L. monocytogenes EGD-e strain was used as the parental strain (detailed informations on the strains used in this study are provided in the key resource table). *L. monocytogenes* strains were grown in brain heart infusion (BHI) medium (Gibco) with shaking at 200 rpm at 37 °C. *E. coli* cells were grown in LB broth. When required, antibiotics were added (chloramphenicol at 35 µg/mL for *E. coli* or 7 µg/mL for *L. monocytogenes,* erythromycin 5 µg/mL for *L. monocytogenes*). LoVo cells were maintained in Ham's F-12K medium (Gibco) supplemented with 20% fetal calf serum and Glutamax (Gibco). Strep-tagged RIG-I, MDA5, LGP2 and mCherry cell lines (Sanchez-Aparicio et al., 2017) were maintained in Dulbecco's modified Eagle medium (Gibco) supplemented with 10% heat-inactivated fetal calf serum (GE Healthcare) and 10,000 U/mL of Penicillin-Streptomycin (Life Technologies) and G418 (Sigma) at 500 µg/mL. The ISRE reporter cell line (STING-37) corresponding to HEK293 cells stably transfected with an ISRE-luciferase reporter-gene was previously described (Lucas-Hourani et al., 2013). All cell lines were maintained and propagated at 37°C with 10% CO_2.

Bacterial mutant generation

For the deletion of *zea*, PCR products comprising ~500 bp upstream and downstream of the zea open reading frame (ORF) were fused *via* splicing by overlap extension PCR and cloned with appropriate restriction sites into the integrative suicide vector pMAD as previously described (Arnaud et al., 2004).

795 **Mice**

796 All animal experiments were approved by the committee on animal experimentation of Institut
797 Pasteur and by the French Ministry of Agriculture. BALB/c mice (8-week-old female) were purchased
798 by Charles River, Inc.

799 **Mice infections**

800 *L. monocytogenes* was thawed from glycerol stocks stored at −80 °C and diluted in phosphate-
801 buffered saline (PBS) before injection. A sublethal dose (10^4 *L. monocytogenes*) was injected into the
802 lateral vein of the tail of each mouse. The number of bacteria in the inoculum was confirmed by
803 plating serial dilutions of the bacterial suspension onto BHI agar plates. For determination of bacterial
804 loads, livers and spleens were recovered and disrupted in PBS at the indicated time points post-
805 infection. Serial dilutions of organ homogenates were plated onto BHI agar plates, and colony
806 forming units (CFUs) were counted after growth at 37 °C for 48 hours.

807 **METHOD DETAILS**

808 **Plasmid vectors and antibodies**

809 Informations about the oligonucleotides used for cloning are provided in the Key Resource Table. To
810 create the plasmids for the overexpression of both full-length ZeaFlag, full-length untagged Zea and
811 Lmo2595, the entire ORFs (with or without a Flag tag at the C terminus for Zea) were synthesized as
812 a gBlocks (Integrated DNA Technologies) and subcloned into the integrative plasmid pAD,
813 downsteam of the *Phyper* promoter (Balestrino et al., 2010). The same strategy was used to generate
814 a plasmid overexpressing ZeaHA (C-terminal HA-tag), but the cloning was subsequently performed
815 in the pP1 plasmid [pAT18 derivative (Trieu-Cuot et al., 1991)]. To create the plasmid for the
816 overexpression of rli143, a fusion fragment corresponding to the entire rli143 gene downstream the
817 *pHyper* promoter was synthesized as a gBlock (Integrated DNA Technologies) and cloned in the pP1
818 plasmid with the appropriate restriction enzymes. To create a plasmid for the overexpression of
819 HisZea in *E. coli* (N-terminal His-tag), the *zea ORF* was amplified by PCR from *L. monocytogenes*

820 genomic DNA and cloned with the appropriate restriction enzymes into the pET28a plasmid,
821 downstream of the polyhistidine tag. To create a plasmid for the overexpression of ZeaFlag in
822 mammalian cells, the cDNA encoding the predicted mature form of Zea was codon-optimized for
823 human expression and synthesized (GeneCust) with a 2xFlag tag at the N-terminus. The resulting
824 construct was then subcloned into pcDNA3.1(+) using the appropriate restriction sites. Modified
825 pCineo plasmid carrying GW cassette (pCineoGW) and the Cherry coding sequence was provided by
826 Dr.Yves Jacob (Institut Pasteur). pEXPR-IBA105-RIG-I and pEXPR-IBA105-mCherry plasmids for
827 the overexpression of Strep-RIG-I and Strep-mCherry, respectively, were previously described
828 (Sanchez David et al., 2016).

829 Anti-Zea polyclonal antibodies were raised against three synthetic peptides spanning the C-terminus
830 of the protein (CSFNAKINVSKGKGKITS; FYSPGLDVKKSKLSKTS; TLKASVSGKKLTTSFK).
831 Two rabbits were injected with each antigen supplemented with Freund's adjuvant (Covalabs,
832 Villeurbanne, France). The total IgG fractions were affinity-purified *via* a resin column containing
833 the antigenic peptide. The affinity-purified antibodies were dialyzed against PBS and 50% glycerol
834 and stored at -20 ˚C.

835 **Bacterial fractionation**

836 For detection of endogenous Zea in culture medium, *L. monocytogenes* was grown to exponential
837 phase (OD_{600} = 1). Bacteria were harvested by centrifugation (4000 × g, 30 min, 4˚ C) and proteins
838 in the culture medium fraction were precipitated by addition of 40% ammonium sulfate and incubated
839 at 4 ˚C (overnight, gentle shaking). Protein were recovered by centrifugation (30 min, 16,000 × *g*, 4˚
840 C) and resuspended in water. Samples were dialyzed against water (overnight, 4 ˚C), concentrated
841 using an Amicon centrifugal filter units (3K cut-off, Millipore) and resuspended in LDS-PAGE
842 sample loading buffer (NuPage, Life Technologies). The bacterial pellet was washed twice in PBS
843 and resuspended in lysis buffer [20mM Tris pH 8.0, 1 mM $MgCl_2$, 150 mM KCl supplemented with
844 protease inhibitors mixture (Complete, EDTA-free, Roche)]. Bacteria were transferred to 2 mL lysing

matrix tubes (MP Biomedicals) and mechanically lysed by bead beating in a FastPrep apparatus (45 s, speed 6.5 three cycles). Subsequently, tubes were centrifuged (10 min at 16,000 × *g*, 4˚ C) to remove cellular debris. To quantify the partition of Zea between bacterial cytosol and culture medium, equal volumes of culture supernatant and bacterial cytosol were analyzed by gradient SDS-PAGE and subjected to Western blotting *via* wet transfer onto 0.45 µm nitrocellulose membrane (Millipore). Detection of overexpressed ZeaFlag in *L. monocytogenes* was performed as described above, except for the protein precipitation from culture medium which was performed as previously described (Archambaud et al., 2005). Briefly, 16% of trichloroacetic acid (TCA) (Sigma) was added to the filtered culture medium and samples were left on ice for 2 hours. Precipitated proteins were recovered by centrifugation (20 min, 16,000 × *g*, 4˚ C). The protein pellets were washed twice with ice-cold acetone and dried at 95 ˚C for 5 min. Proteins were resuspended in NuPage LDS sample buffer and an equal percentage of bacterial cytosol and culture medium were subjected to western blotting as above.

Expression and purification of HisZea

pET28a-HisZea (described above) was used to transform *E. coli* C43 bacteria which were grown at 37 °C in Terrific broth (TB) (Thermo Fisher Scientific) supplemented with 50 µg/mL kanamycin. Expression was induced by the addition of IPTG to a final concentration of 1 mM at OD_{600nm} = 0.7 AU. Cultures were incubated overnight, and cells were harvested by centrifugation (5,500 × *g*, 20 min, 4 °C). The bacterial pellet was resuspended in Buffer A (50 mM potassium phosphate pH 7.0, 300 mM NaCl, 10 % glycerol, 20 mM imidazole, 2 mM beta-mercaptoethanol). All subsequent steps were performed at 4 °C. Cell lysis was carried out by passing the samples three times through a pre-cooled microfluidizer operating at 17,000 psi. The soluble fraction was then obtained by centrifugation at 39,000 × *g* for 45 minutes at 4 °C. Subsequently, the supernatant was loaded onto a pre-equilibrated Ni-NTA column (Qiagen) at 0.5 mL/min with a peristaltic pump at 4 °C. The washing and elution steps were performed on an AKTA system using steps of 35 % and 100 % Buffer

B (50 mM potassium phosphate pH 7.0, 300 mM NaCl, 10 % glycerol, 300 mM imidazole, 2 mM beta-mercaptoethanol). The fractions containing Zea were pooled, concentrated with an Amicon centrifugal filter unit (10K cut-off, Millipore), and further purified by size-exclusion chromatography on a Hi Load S200 10/300 column (GE Healthcare) pre-equilibrated in Buffer C (50 mM potassium phosphate pH 7.0, 300 mM NaCl, 10% glycerol, 2 mM beta-mercaptoethanol). Peak fractions were pooled, concentrated to 10 mg/mL, and subsequently dialyzed against Buffer D (50 mM potassium phosphate pH 7.0, 100 mM NaCl, 10% glycerol, 2 mM beta-mercaptoethanol). After dialysis, protein concentration was assessed again and the sample was flash-frozen in liquid nitrogen. During purification, the purity and homogeneity of the sample were monitored by SDS-PAGE.

RNA extraction

Total RNA from *L. monocytogenes* was extracted as previously described (Mellin et al., 2013). Briefly, bacteria grown either to exponential phase (OD_{600nm} = 0.8-1.0 for growth cultures in BHI or OD_{600nm} = 0.4 for growth cultures in MM) or stationary phase (overnight culture: OD_{600nm} = 3.0-3.5 for growth cultures in BHI, or OD_{600nm} = 1.0 for growth cultures in MM) were pelleted by centrifugation (2862 × *g*, 20 min, 4 ˚C). Pellets were resuspended in 1 mL TRIzol Reagent (Ambion), transferred to 2 mL Lysing Matrix tubes and mechanically lysed by bead beating in a FastPrep apparatus (45 s, speed 6.5 followed by an additional 30 s, speed setting 6.5). Subsequently tubes were centrifuged (5 min at 8,000 × *g*, 4 °C) in a tabletop centrifuge and lysates were transferred to a 2 mL Eppendorf tube. RNA isolation proceeded according to the manufacturer's instructions. Briefly, 200 µL of chloroform (Sigma) were added to the lysate, shaken and incubated for 10 min at room temperature, followed by centrifugation (15 min at 13,000 × *g*, 4 °C). The upper aqueous phase was removed and transferred to a new 1.5 mL Eppendorf tube and RNA was precipitated by the addition of 500 µL isopropanol and incubation at room temperature for 5– 10 min. RNA pellets (10 min at 13,000 × *g*, 4 °C) were washed twice with 75% ethanol and resuspended in 50 µL of nuclease-free water (Ambion).

To extract total secreted RNA from MM, *L. monocytogenes* was grown until exponential phase (OD_{600nm} = 0.4). Medium was recovered by centrifugation (2862 × *g*, 20 min, 4 ˚C), filtered (0.22 µm) and concentrated 10 times using an Amicon centrifugal filter unit (3K cut-off). Medium was then brought back to the initial volume by adding nuclease-free water and concentrated again. This desalting process was repeated three times to avoid co-precipitation of salts during the subsequent RNA isolation. RNA was then extracted twice with acid phenol/chloroform, precipitated with ethanol/0.3 M sodium acetate and resuspended in nuclease-free water.

RNA extraction from LoVo cell monolayers in 6-well plates was performed by using TRIzol Reagent. Briefly, cells were washed once with ice-cold PBS and directly lysed in the well by adding 1 mL of TRIzol and gentle pipetting. Samples were vortexed thoroughly for 30 s before the addition of 200 µL chloroform and then incubated 3 min at room temperature. After centrifugation (15 min, 12 000 × *g*, at 4 °C), the upper aqueous phase was transferred to a new Eppendorf tube and RNA was precipitated by the addition of an equal volume of isopropanol and incubation at room temperature for 10 min. RNA pellet was washed twice with 70% ethanol and resuspended in 50 µL of nuclease-free water.

In vitro RNA transcription

cDNA templates of the *L. monocytogenes* small RNAs fused with a T7 promoter were obtained by PCR amplification from genomic DNA with the appropriate primers. The cDNA quality was verified on a 1% agarose gel and visualized by ethidium bromide staining. cDNA was purified from agarose gel with a Gel extraction kit (Qiagen) and resuspended in nuclease-free water. Purified cDNA (200 ng) was transcribed *in vitro* by using the MAXIscript T7 *in vitro* transcription kit (Invitrogen) according to the manufacturer's recommendation. The quality of the *in vitro*-transcribed RNA was verified by SYBR Gold (Life Technologies) staining after running on 6% Novex™ TBE-Urea gel (Thermo Fisher Scientific) or by the Bioanalyser RNA nano kit (Agilent). The p2RZ vector expressing a part of Cherry protein transcript was described elsewhere (Chazal et al., 2018) and

linearized by XhoI before performing *in vitro* transcription, as described above. The biotinylated small RNAs were also *in vitro*-transcribed as above, except that 0.35 mM of biotin-16-UTP (Roche) was included in the reaction mixture.

Electrophoretic mobility gel shift assay (EMSA)

In vitro formation of HisZea - RNA complexes was assessed by electrophoretic mobility gel shift assay (EMSA). For *in vitro* RNA synthesis, 1 µg of cDNA template carrying a T7 promoter was amplified by PCR and *in vitro*-transcribed using the MAXIscript T7 *in vitro* transcription kit according to the manufacturer's instructions. The quality of the *in vitro*-transcribed RNA was verified as described above. RNA was purified and concentrated using "RNA clean & concentrator" (Zymo research) before dephosphorylation and 5'-end labeling as previously described (Chevalier et al., 2009). Labelled RNA was denatured for 1 min at 95 °C, chilled on ice (5 min) and renatured by slowly cooling down to 25 °C. Upon addition of HisZea (concentrations as indicated in the figure legends) the complex was formed in 20 µL of binding buffer [50 mM Tris pH 8.0, 300 mM NaCl, 10% glycerol, 50 µg/mL fatty acid-free BSA (Roche), supplemented with 1 µg of yeast tRNA (Invitrogen)] for 20 min at room temperature. Unlabeled competitor was added and samples were incubated for an additional 20 min. Samples were mixed with loading buffer (50% glycerol, 0.5% tris-borate EDTA and 0.1% xylene cyanol) before running on native 8% Novex™ TBE gels (Thermo Fisher Scientific). Signals were detected by autoradiography (at least one-hour exposure at -80 °C in presence of an intensifying screen).

Biotin pull-down assay

HisZea (2.5 µg) was incubated with 50 µL of equilibrated streptavidin magnetic beads (BioLabs) in 250 µL of binding buffer (150 mM KCl, 25 mM Tris pH 8.0, 5 mM EDTA, 0.5 mM DTT, 0.5% NP40) for 45 min at 4 ˚C with shaking. Beads were recovered by centrifugation (500 × *g*, 5 min, 4 ˚C) and discarded. The HisZeap-containing supernatant was used in the subsequent steps. This preclearing step was performed in order to remove the Zea fraction which aggregated non-specifically

945 onto the beads. Biotinylated RNA (500 nM) was added to the HisZea-containing supernatant and
946 incubated for 30 min, 4 ˚C with shaking. Then, 50 µL of equilibrated streptavidin magnetic beads
947 were added for a further incubation (30 min, 4 ˚C with shaking). The beads were then washed four
948 times in binding buffer and bound HisZea was recovered by addition of NuPage LDS sample buffer.

949 **RNase protection assay**

950 Equimolar concentrations of HisZea or GST (1 µM) were mixed with ^{32}P radiolabelled rli143 in 20
951 µL of binding buffer (50 mM Tris pH 8.0, 300 mM NaCl, 10% glycerol and 50 µg/mL fatty acid-free
952 BSA) and incubated at 25 ˚C for 30 min. Then, 0.0033U of RNaseI (Ambion) were added before
953 incubation for either 1 or 3 min at 37 ˚C. Reactions were stopped by addition of NuPage LDS sample
954 buffer and samples were loaded on 8% Novex^{TM} TBE-Urea gels (Thermo Fisher Scientific). Signals
955 were detected by autoradiography (at least one-hour exposure at -80 °C in presence of an intensifying
956 screen).

957 **Immunoprecipitations**

958 To assess the interaction between ZeaFlag and ZeaHA, 25 mL of *L. monocytogenes* overnight cultures
959 expressing either ZeaFlag alone, or both ZeaFlag and ZeaHA were centrifuged (2862 × *g*, 20 min, 4
960 ˚C) to collect bacteria and culture medium. The recovered medium was filtered by using Millex-GP
961 0.22 µm filters (Millipore), supplemented with 0.2% of Triton X100, before adding 20 µL of M2 Flag
962 magnetic beads (Sigma). Samples were shaken for 2 hours at 4 ˚C and then washed four times with
963 lysis buffer (20mM Tris pH 8.0, 1 mM $MgCl_2$, 150 mM KCl, supplemented with protease inhibitors
964 mixture). The immunoprecipitated material was finally eluted using 100 µg/mL of 3xFlag peptide
965 (Sigma) according to the manufacturer's instructions. Bacterial pellet was washed twice in ice-cold
966 PBS, resuspended in lysis buffer and lysed in a FastPrep apparatus (45 s, speed 6.5, thrice). The
967 samples were then clarified by centrifugation (14000 × *g*, 10 min, 4 ˚C, twice) and protein
968 concentration determined by Bradford assay. The same percentage of bacterial cytosol compared to
969 the culture medium was used to immunoprecipitate ZeaFlag, under the same condition used for the

culture medium. Equal amounts of eluted proteins were subjected to western blotting *via* wet transfer onto a 0.45 µm nitrocellulose membrane.

To assess the interaction between ZeaFlag and Strep-RIG-I, 25 mL of culture medium from *L. monocytogenes wt* and *zea^{Flag}-pAD* overnight cultures were recovered by centrifugation (2862 × *g*, 30 min, 4 ˚C) and filtered by using Millex-GP 0.22-µm filters. Filtered culture medium was supplemented with 0.2% Igepal. Then, 25 µL of M2 Flag magnetic beads were added and samples were incubated overnight at 4 ˚C with shaking. Magnetic beads were recovered and washed four times with washing buffer (20 mM MOPS-KOH pH 7.4, 120 mM KCl, 0.2% Igepal, 2 mM beta-mercaptoethanol) and left on ice while preparing the cell lysate. HEK293 cells stably transfected with Strep-RIG-I were lysed in lysis buffer [20 mM MOPS-KOH pH 7.4, 120 mM KCl, 0.2% Igepal, 2 mM beta-mercaptoethanol, supplemented with a protease inhibitors mixture and 12.5 U/µl RNasin (Promega)], sonicated twice for 15 sec at 20% amplitude and incubated on ice for 30 min. The cell lysate was cleared by centrifugation (14000 × *g*, 10 min, 4 ˚C) with the supernatant assayed for protein concentration with Bradford assay and used fresh. At least 1 mg of cell lysate was added to the Zea-containing washed Flag magnetic beads (prepared above) and incubated overnight at 4˚ C with shaking. Beads were washed four times in washing buffer and twice in washing buffer without Igepal. For RNaseA treatment, 100 µg/mL of RNaseA (Roche) in lysis buffer without Igepal were added to the beads (30 min, ice) followed by two further washes in the same buffer. Zea was eluted from the magnetic beads with 3xFlag peptide at 100 µg/mL, according to the manufacturer's recommendations, in a total volume of 50 µL. Samples were then subjected to western blotting *via* wet transfer onto a 0.45-µm nitrocellulose membrane.

For ZeaFlag immunoprecipitation from mammalian cells, LoVo cells in 10-cm^2 dishes were transiently co-transfected with 7 µg of each DNA (ZeaFlag and Strep-RIG-I) using 24 µL of Lipofectamine LTX (Thermo Fisher Scientific). 24 hours after transfection, the cells were washed twice with PBS and lysed using 1 ml lysis buffer per dish (20 mM MOPS-KOH pH 7.4, 120 mM

KCl, 0.2% Igepal, 2 mM beta-mercaptoethanol, supplemented with protease inhibitors mixture). The lysate was sonicated for 15 sec, at 20% amplitude and incubated on ice for 30 min with shaking. The lysate was then clarified (13,000 × *g*, 10 min, 4 ˚C) and assayed for protein concentration (Bradford). 0.5 mg of total lysate was incubated with 15 µL of M2 Flag magnetic beads (overnight, 4 ˚C, shaking). Beads were recovered and washed three times in lysis buffer before treatment with RNase and elution with the 3xFlag peptide (both performed as above). Samples were then subjected to western blotting *via* wet transfer onto a 0.45-µm nitrocellulose membrane.

For Hfq immunoprecipitation, bacteria were grown in 20 mL of BHI until stationary phase and pelleted (2862 × *g*, 30 min, 4 ˚C). The bacterial pellet was washed twice with ice-cold PBS and mechanically lysed in 1 mL of lysis buffer (20 mM Tris pH 8.0, 1 mM $MgCl_2$, 150 mM KCl, 1 mM DTT, supplemented with protease inhibitors) in 2 mL Lysing Matrix tubes by bead beating in a FastPrep apparatus (45 s, speed 6.5, thrice). Bacterial lysate was clarified by centrifugation (18407 × *g,* 20 min, 4 ˚C) and protein concentration was determined by Bradford assay. The culture medium was filtered by using Millex-GP 0.22-µM filters and supplemented with 0.2% Igepal. 10 µl of anti-Hfq anti-serum were added to an equal percentage of bacterial cytosol and culture medium and incubated overnight at 4 ˚C under shaking condition. Then, 50 µl of protein A Sepharose beads (GE Healtcare) were added for a further hour of incubation (4 ˚C, shaking). The immune complexes were collected by centrifugation (500 × *g*, 5 min, 4 ˚C). After three washes with lysis buffer, the bound protein was eluted from the protein A Sepharose beads by boiling (10 min) in 50 µl LDS sample buffer.

For immunoprecipitation of ZeaFlag from nuclear and cytosolic fractions of infected LoVo cells (6 hours, MOI 50), 20 µl of pre-equilibrated M2 Flag magnetic beads were added to equal percentage of cytosolic and nuclear fractions. Samples were incubated overnight at 4 ˚C with shaking. After three washes in lysis buffer (20 mM Tris pH 8.0, 150 mM NaCl, 1 mM DTT, 1% Igepal), immune

complexes were retrieved by adding 100 mg/mL of 3xFlag peptide. Samples were then subjected to western blotting *via* wet transfer onto a 0.45-µM nitrocellulose membrane.

Immunofluorescence

Immunofluorescence was performed as previously described (David et al., 2018).

Cell fractionations

Fractionation of cultured cell lines was performed as previously described (Pereira et al., 2018).

Live/dead bacterial staining

L. monocytogenes was grown in 20 mL of BHI until stationary phase. Bacteria were pelleted (2862 × *g*, 20 min, room temperature) and then stained with *LIVE/DEAD BacLight* (Molecular Probes), following the manufacturer's recommendation. Bacterial suspension (20 µL) was then deposited on a glass coverslip and immediately imaged by using a Zeiss AxioObserver.Z1 inverted fluorescence microscope equipped with an Evolve EM-CCD camera (Photometrics). Images were acquired with a 100× N.A. 1.4 oil objective using MetaMorph.

RIP-Seq

50 mL *Δzea+zea-pAD L. monocytogenes* stationary phase (OD_{600nm} = 3.5) culture (a zea-deletion strain in which one copy of the zea gene was integrated in the *L. monocytogenes* genome under the control of a constitutive promoter) was centrifuged (2862 × *g*, 20 min, 4 ˚C) to recover the culture medium and the bacterial pellet. 10 mL culture medium were filtered (0.22-µm) and concentrated to 1 mL by using Amicon centrifugal filter unit (3K cut-off). Concentrated medium was then supplemented with 0,05% of Triton X100, centrifuged again (18407 × *g,* 20 min, 4 ˚C) and left on ice while preparing bacterial cytosolic extracts. The bacterial pellet was washed thrice in ice-cold PBS and lysed by mechanical shaking in a FastPrep apparatus (described above) in 1 mL of lysis buffer (25mM Tris pH 7.4, 150mM KCl, 1mM DTT, 0.05% Triton X100) supplemented with protease inhibitors mixture. Bacterial cytosol was recovered by centrifugation (two serial

centrifugations at 18407 × *g,* 20 min, 4 ˚C) and protein concentration determine by Bradford assay. One-milliliter of bacterial cytosol and concentrated culture medium (corresponding to 50 mL and 10 mL of the bacterial cytosol and culture medium, respectively) were individually loaded on a Superose 6 10/300 GL column pre-equilibrated with lysis buffer without Triton X100. About 161 fractions of 220 µL were collected, and one out of every seven fractions was concentrated by acetone precipitation and the presence of Zea and EF-Tu analyzed by western blotting after wet transfer onto a nitrocellulose membrane. Fractions containing the complexes (A or B) were then pooled and processed for immunoprecipitation assays. Briefly, each sample was incubated overnight at 4 ˚C with shacking, with a mix of 30 µg of anti-Zea antibodies (10 µg of each antibody) or 30 µg of normal rabbit IgG (CellSignaling) . Then, 50 µL of Protein A Sepharose were added for further 2 hours to recover immunocomplexes. The beads were washed four times with lysis buffer and treated with Turbo DNase (Ambion) for 10 min at 37 ˚C in 200 µL 1X Turbo DNase buffer. Samples were vortexed for 30 s after the addition of 200 µL of acid phenol (Ambion). Then, 50 µL chloroform (Sigma) were added and samples were centrifuged for 5 min at 10 000 × *g* at 4 ˚C. The aqueous upper phase was recovered and transferred to a new Eppendorf tube. RNA was precipitated by adding the same volume of isopropanol and 0.3 M of sodium acetate (Ambion) and 1 µL of glycogen (Invitrogen). Samples were centrifuged (30 min, 10 000 × *g*, 4 ˚C), and RNA was washed once with 70% ethanol before being resuspended in 25 µL of nuclease-free water. RNA was analyzed with the Bioanalyser RNA pico kit (Agilent). Purified RNA was fragmented with the "RNA fragmentation reagents" (Thermofisher), purified by ethanol precipitation and quality-controlled with the Bioanalyser, as described above. Directional RNA-seq libraries were prepared with 30 ng of purified RNA for each sample by using NEBNext Multiplex Small RNA Library Prep Set for Illumina (New England Biolabs) according to the manufacturer's instructions. When required, the RNA samples were spiked-in with a synthetic *in vitro*-transcribed AdML splicing reporter (Allemand et al., 2016)

in order to have 30 ng of total RNA. Libraries were sequenced on an Illumina HiSeq 2500 platform (SR100).

RIP-Seq data analysis

The *L. monocytogenes* EGD-e genome (NC_003210) and a list of 3160 transcripts (genes, small-RNAs, tRNAs, and rRNAs) were downloaded from the Listeriomics database(Becavin et al., 2017). After the sequencing of all RIP-Seq samples, the resulting reads were trimmed (AlienTrimmer 0.4.0, default parameters) (Criscuolo and Brisse, 2013). They were mapped on the EGD-e genome using Bowtie2 2.1.0 (very-sensitive parameter) (Langmead and Salzberg, 2012). Mapping files were filtered to keep uniquely mapped reads using SAMtools 0.1.19 (*samtools view -b –q 1* parameters) (Li et al., 2009), and saved to BAM files after indexation. Read Per Million coverage files were saved in BigWig format using bamCoverage package from deepTools 3.1.3 (Ramirez et al., 2016). The quality of the sequencing and mapping was assessed using FastQC 0.10.1 and MultiQC 0.7 (Ewels et al., 2016). The number of reads per transcript (mRNA, sRNA, tRNA, rRNA) was counted using FeatureCount (1.4.6-p3 default parameters) (Liao et al., 2014). Statistical analysis was performed using SARTools package (Varet et al., 2016) and in-house R scripts (https://gitlab.pasteur.fr/hub/ripseq-listeria). Data were normalized with the TMM (Robinson et al., 2010) (edgeR package) normalization method. Finally, the $\log_2$(Fold changes) were calculated by subtraction of $\log_2$(TMM) normalized expression values.

Sequencing of total secreted *L. monocytogenes* RNA

To extract total secreted RNA from the culture medium, *L. monocytogenes* strains (*wt* and *Δzea+zea-pAD)* were grown to exponential phase (OD_{600nm} = 0.4) in 14 mL of MM under microaerophilic conditions using Oxoid™ AnaeroGen™ 2.5L gas packs (Thermo Fisher) at 25 °C. Under this condition *zea* appeared slightly up-regulated compared to standard growth conditions (i.e 37 °C, BHI medium) (Becavin et al., 2017). A parallel culture (same conditions) was set-up to check the OD and arrest the bacterial growth when the strains reached the same OD. The culture medium was then

recovered by centrifugation (2862 × *g*, 20 min, 4 ˚C) and filtered (0.22 µm). The bacterial pellet was stored at -80 ˚C for subsequent RNA extraction. 10 mL of the filtered culture medium were desalted and the RNA was extracted as described above. The quality of the RNA was checked by using the Bioanalyser RNA nano kit. The amount of recovered RNA was similar in all the samples. Total secreted RNA (5 µg) was ribodepleted by using the Ribo Zero rRNA removal kit (Illumina) following the manufacturer's instructions. Ribodepletion was controlled by the Bioanalyser RNA pico kit. Directional RNA-seq libraries were prepared with 100 ng of purified RNA for each sample by using NEBNext Multiplex Small RNA Library Prep Set for Illumina according to the manufacturer's instructions. Libraries were sequenced on an Illumina NextSeq500 platform (SR75).

Sequencing analysis of total secreted *L. monocytogenes* RNA

The RNA-seq datasets were first trimmed to keep only reads longer than 45bp (AlienTrimmer 0.4.0, *-l 45*) (Criscuolo and Brisse, 2013). They were mapped on the EGD-e genome using Bowtie2 2.1.0 (very-sensitive parameter) (Langmead and Salzberg, 2012). Mapping files were filtered to keep uniquely mapped reads using SAMtools 0.1.19 (*samtools view -b –q 1* parameters) (Li et al., 2009), and saved to BAM files after indexation. Read Per Million coverage files were saved in BigWig format using bamCoverage package from deepTools 3.1.3 (Ramirez et al., 2016). The quality of the sequencing and mapping was assessed using FastQC 0.10.1 and MultiQC 0.7(Ewels et al., 2016). The number of reads per transcript (mRNA, sRNA) was counted using HTSeq 0.9.1*(-s no -m union --nonunique all* parameters) (Anders et al., 2015). Differential analysis was performed using SARTools(Varet et al., 2016) and DESeq2 R(Love et al., 2014) packages

RIP-qPCR

L. monocytogenes bacterial cultures (*Δzea+zea-pAD* strain*)* were processed essentially as described for the RIP-seq experiment unless otherwise stated. In summary, *L. monocytogenes* was grown until the stationary phase (OD_{600nm} = 3.5) and, for every sample, 50 mL of bacterial culture were processed as follows. Bacteria were pelleted at 2862 × *g*, 20 min, 4 ˚C and culture supernatant was filtered and

processed (5 mL) for total RNA purification (input, 10%), by performing two sequential phenol/chloroform extractions followed by ethanol/sodium acetate precipitation. The RNA pellet was washed once with ethanol 70% and resuspended in 20 µL nuclease-free water. Purified RNA was then treated with Turbo DNase and purified again, as described above. The remaining medium (45 mL, 90% of the initial sample) was processed for Zea immunoprecipitation. Briefly, 20 µg of a mix of Zea antibodies (6.6 µg of each antibody) were coupled to 100 µl of Protein A Dynabeads (Invitrogen) for 2 hours in 500 µl of PBS (room temperature, shaking). Beads were then washed twice with PBS and once with lysis buffer (25mM Tris pH 7.4, 150mM KCl, 1mM DTT, 0.05% Triton X100). Culture medium was supplemented with 0.05% Triton X100 before the addition of the anti-Zea antibody-coupled beads. Samples were then incubated overnight (4 ˚C, shaking). Beads were washed four times with lysis buffer, treated with Turbo DNase and processed for RNA extraction. Purified RNA was stored at -80 ˚C until use. The bacterial pellet was washed thrice in ice-cold PBS and then mechanically lysed by using FastPrep apparatus in 1 mL of lysis buffer supplemented with protease inhibitors mixture and RNasin (Promega) at 12.5 U/µL. Bacterial lysate was clarified by two sequential centrifugations and the final volume was carefully measured. A volume corresponding to 10% of the total sample (input) was treated with DNase and processed for RNA isolation by phenol/chloroform extraction and ethanol/sodium acetate precipitation. Purified RNA was resuspended in nuclease-free water and stored at -80 ˚C until use. The remaining bacterial cytosol was incubated with an anti-Zea antibody coupled to Protein A as described above (overnight, 4 ˚C, shaking). Beads were washed four times with lysis buffer, treated with Turbo DNase and processed for RNA extraction. For qPCR analysis, 100 ng of purified RNA were subjected to reverse transcription in 20 µL final volume using the Reverse Transcription Kit (Qiagen) according to the manufacturer's instructions. Reactions were then diluted by adding 180 µL of nuclease-free water. qPCR was assayed in 10 µl reactions with Brillant III Ultra Fast SYBR-Green qPCR Master Mix (Agilent). Reactions were carried out in a Stratagene MX3005p system with the following thermal

profile: 5 min at 95 °C, 37 cycles of 10 s at 95 °C and 12 s at 60 °C. Results were analyzed with an MxPro software, as described earlier (Batsche et al., 2006).

Quantitative real-time PCRs

For qPCR of *L. monocytogenes* secreted RNA (phage, lma-monocin and rli143 RNAs), bacterial strains were grown in MM until exponential phase (OD_{600nm} = 0.4). *L. monocytogenes wt*, *Δzea* and *Δzea+zea-pAD* strains were used for the phage and lma-monocin quantification; *L. monocytogenes wt*, *Δzea*, *zea-pAD* and *lmo2595-pAD L. monocytogenes* strains were used for the quantification of rli143; *L. innocua wt*, *zea-pAD* and *lmo2595-pAD* strains were employed for the quantification of rli143. The bacterial OD was measured and the cultures were recovered when OD was equal for all the strains. MM was collected by centrifugation, filtered and processed for RNA extraction (as described above). Purified RNA (5-10 µg) was subjected to DNase treatment using the DNase treatment and removal kit (Ambion). Treated RNA (500 ng) was mixed with an equal amount of CleanCap™ OVA mRNA (TriLink) which serves as an internal control for normalization, and processed for reversed transcription and qPCR, as above. Gene expression levels were normalized to the OVA mRNA, and the fold change was calculated using the ΔΔCT method.

For qPCR of *Listeria* genes from total (intracellular) *L. monocytogenes* RNA, the RNA was extracted, as described in the RNA extraction section and treated, as described above, except that the OVA mRNA was not included in the reverse transcription reaction. Gene expression levels were normalized to the *rpob* gene, and the fold change was calculated using the ΔΔCT method.

For qPCR of Hfq-associated RNAs, RNA was extracted from immunoprecipitated Hfq, by using the protocol described for the RIP-seq of Zea. DNase-treated RNA (120 ng) was subjected to reverse transcription. Gene expression levels were normalized to the input fractions, and the fold change was calculated using the ΔΔCT method.

For qPCR of IFNβ, IFNγ and IL-8, mammalian RNA was extracted, as described in the RNA extraction section. Purified RNA (5-10 µg) was subjected to DNase treatment, and 1 µg processed for reverse transcription, as described above. Gene expression levels were normalized to the actin mRNA and to the uninfected samples, and the fold change was calculated using the ΔΔCT method.

Purification of RLR complexes and RNA extraction.

Four 15-cm^2 tissue culture dishes per cell line were pretreated with 0.1 mg/mL poly-L-Lysine-hydrobromide (Sigma), rinsed with distilled water and dried for 1 hour before plating the cells. Cells (30-40x10^6) were plated per dish in 20 mL of DMEM medium for 24 hours before infection. Overnight *L. monocytogenes* EGD-e cultures in BHI were diluted 1/20 in fresh BHI the day of infection and grown up to OD_{600nm} = 1. Each plate was infected with an MOI of 50 for 1 hour before replacing the media with complete DMEM containing 10 µg/mL of gentamicin to kill extracellular bacteria. After an additional 3 hours (in total 4 hours of infection), plates were rinsed twice with ice-cold PBS, crosslinked at 400 mJ/cm^2 in 10 mL of ice-cold PBS/plate and cells were then scraped, pelleted and resuspended in 8 mL of MOPS lysis buffer (20 mM MOPS-KOH pH 7.4, 120 mM KCl, 0.5% Igepal, 2 mM beta-mercaptoethanol, supplemented with protease inhibitors mixture and RNasin at 0.2 U/µl and protease inhibitors mixture (Roche). Cell lysates were incubated on ice for 20 min with gentle mixing every 5 min and then clarified by centrifugation at 16000 × *g* for 15 min at 4 ˚C. Streptactin Sepharose beads (GE Healthcare, 100 µL/dish) were washed in MOPS washing buffer (20 mM MOPS-KOH pH 7.4, 120 mM KCl, 2mM beta-mercaptoethanol, supplemented with RNasin 0,2 U/µL and protease inhibitors mixture and finally resuspended in 1 mL of MOPS lysis buffer per initial culture dish. Clarified cell lysate was incubated with Streptactin beads for 2 hours at 4 °C. The beads were washed three times with MOPS washing buffer and centrifuged at 1600 × *g*, 5 min at 4°C. Strep-tagged proteins were then eluted twice for 15 min at 4 °C in 250 µL/dish of 1X elution buffer (IBA, Biotin Elution Buffer 10X). Each sample was treated with proteinase K (Roche) in v/v of 2X proteinase K buffer (200 mM Tris pH 8, 100 mM NaCl, 20 mM EDTA, 4M urea) for 20 min at 4 °C

that has been preincubated 20 min at 37 °C to remove RNase contamination. RNA purification was performed using TRI Reagent LS (Sigma). RNA was dissolved in 50 µL of DNase-free and RNase-free ultrapure water. Extracted RNAs were analyzed using Nanovue (GE Healthcare) and Bioanalyser RNA nano kit (Agilent) before being processed for next-generatio sequencing (HiSeq 2500, SR50).

Data analysis of RLR-associated RNAs

Due to the high number of eukaryotic RNAs in the datasets and presence of insertions and deletions, the reads were trimmed (AlienTrimmer 0.4.0) (Criscuolo and Brisse, 2013), and mapped using GSNAP (v2018-07-04) (Wu et al., 2016), a special mapping software allowing variability in reads sequence. Mapping files were filtered to keep uniquely mapped reads using SAMtools 0.1.19 (*samtools view -b –q 1* parameters) (Li et al., 2009), and saved to BAM files after indexation. Read Per Million coverage files were saved in BigWig format using bamCoverage package from deepTools 3.1.3 (Ramirez et al., 2016). The quality of the sequencing and mapping was assessed using FastQC 0.10.1 and MultiQC 0.7 (Ewels et al., 2016). The number of reads per transcript (mRNA, sRNA, tRNA, rRNA) was counted using HTSeq 0.9.1*(-s no -m union --nonunique all* parameters) (Anders et al., 2015). Differential analysis was performed using SARTools (Varet et al., 2016) and EdgeR packages (Robinson et al., 2010) (https://gitlab.pasteur.fr/hub/ripseq-listeria).

Immunostimulatory activity of Zea-interacting small RNAs

The ISRE reporter cells (STING-37 cell line) (Lucas-Hourani et al., 2013) were seeded in 24-well plates and 2 hours later transfected with 100 ng of *in vitro*-transcribed rli143, rli18, rli92 and 250 nucleotides-long fragments of mCherry RNAs (Chazal et al., 2018) using Lipofectamine 2000 (Thermofisher Scientific). 100 ng of high molecular weight (HMW, tlrl-pic, Invivogen) and low molecular weight Poly(I:C) (LMW, tlrl-picw, Invivogen), and 100 ng of short 5'3P RNA (produced as previously described (Lucas-Hourani et al., 2013)) were used as positive controls. Cells were lysed 24 hours post-transfection with 200 µL Passive Lysis buffer (Promega). The Firefly luciferase activity

was measured using the Bright-Glo Luciferase Assay System (Promega) following the manufacturer's recommendation.

Statistical analysis

All data are expressed as mean and standard error of the mean. Student's t-test was used for statistical analysis. Differences in means were considered statistically significant at $p < 0.05$. Significance levels are: * $p < 0.05$; ** $p < 0.01$; *** $p < 0.001$. Sample number (n) indicates the number of independent biological samples in each experiment, for each set of experiments this information is provided in the figure legends.

DATA AND SOFTWARE AVAILABILITY

RIP-Seq, RNA-seq and RLRs purification and sequencing data have been deposited in the ArrayExpress database at EMBL-EBI (www.ebi.ac.uk/arrayexpress) under accession number E-MTAB-7665. All scripts used for the analysis have been deposited on the Institut Pasteur GitLab: https://gitlab.pasteur.fr/hub/ripseq-listeria

1227

1228

Figure 1

A

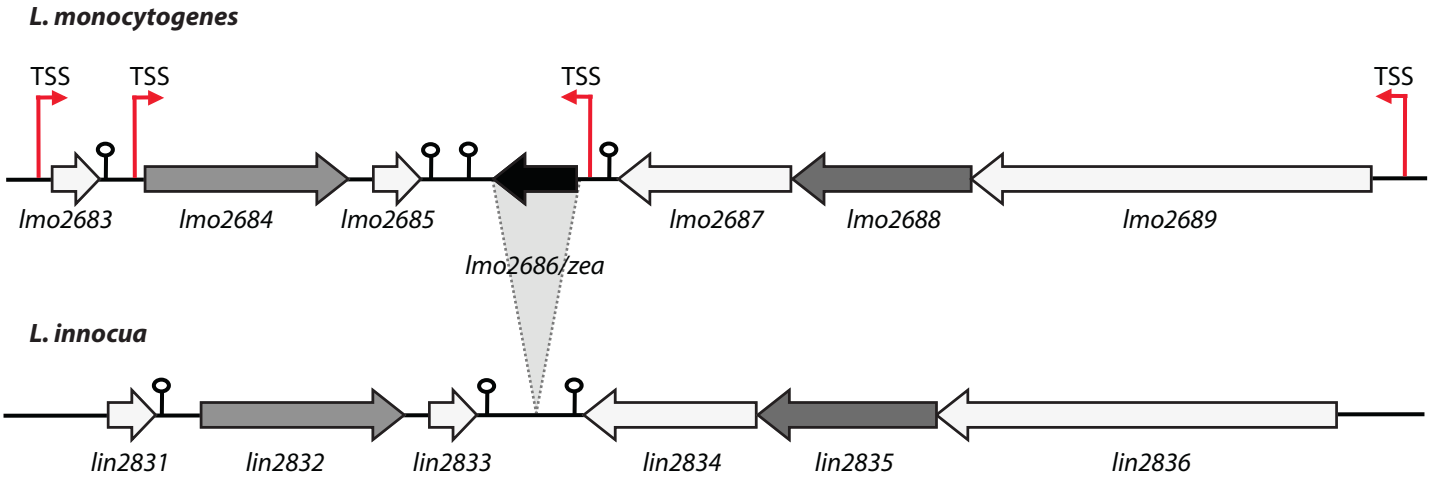

B

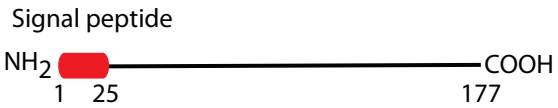


```
        10         20         30         40         50
MKEFLFFAVF TFIMTIGVGV INASASEIEN PDNIQEAEVE TFDLNGNIAQ
        60         70         80         90        100
EKEIVLEDGT EGTLGVMPII DERPLLKGTY SLANGTSTWK IYWYSGVYNC
       110        120        130        140        150
SFNAKINVSK GKGKITSAYN PWYQFYSPGL DVKKSKLSKT SSGSSASYVF
       160        170
DCKNKISNWN VTLKASVSGK KLTTSFK
```

C

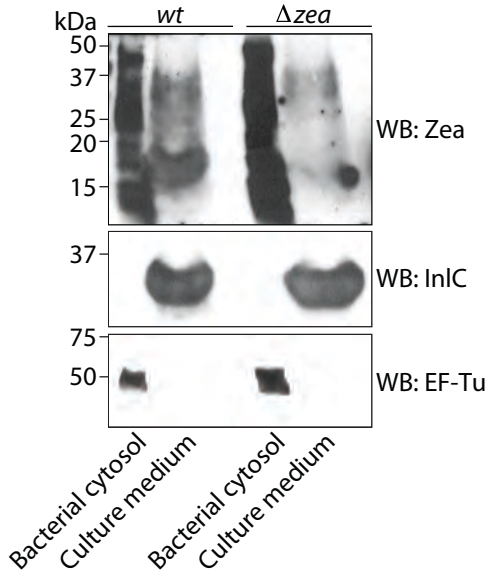

D

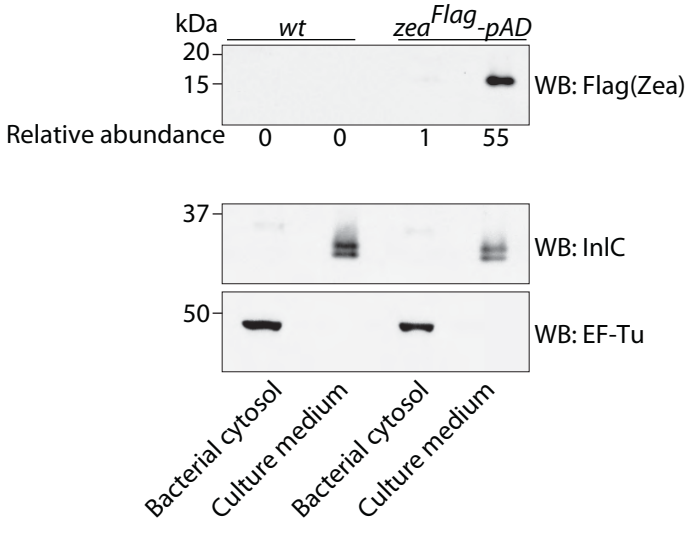

Figure 2

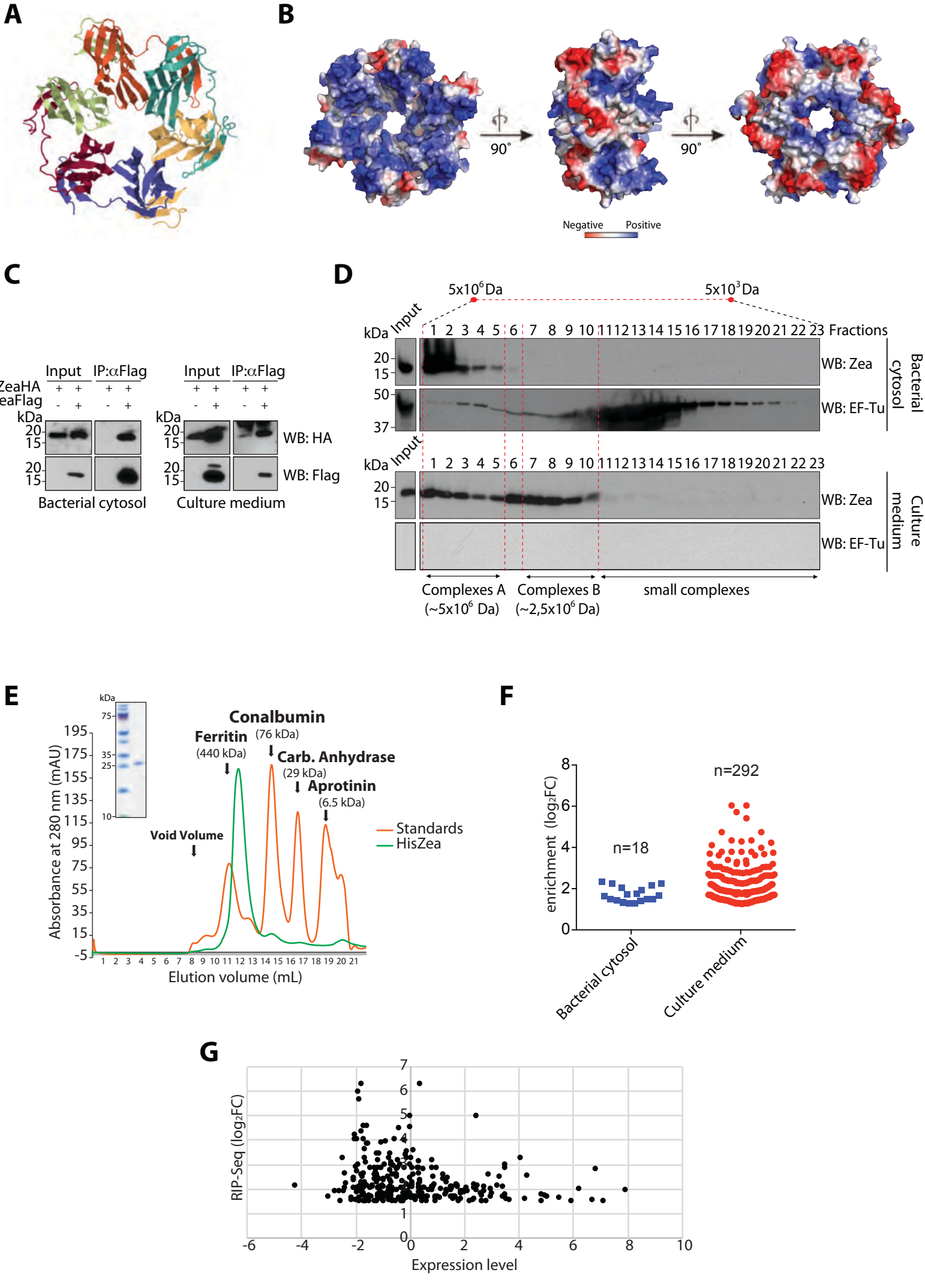

Figure 3

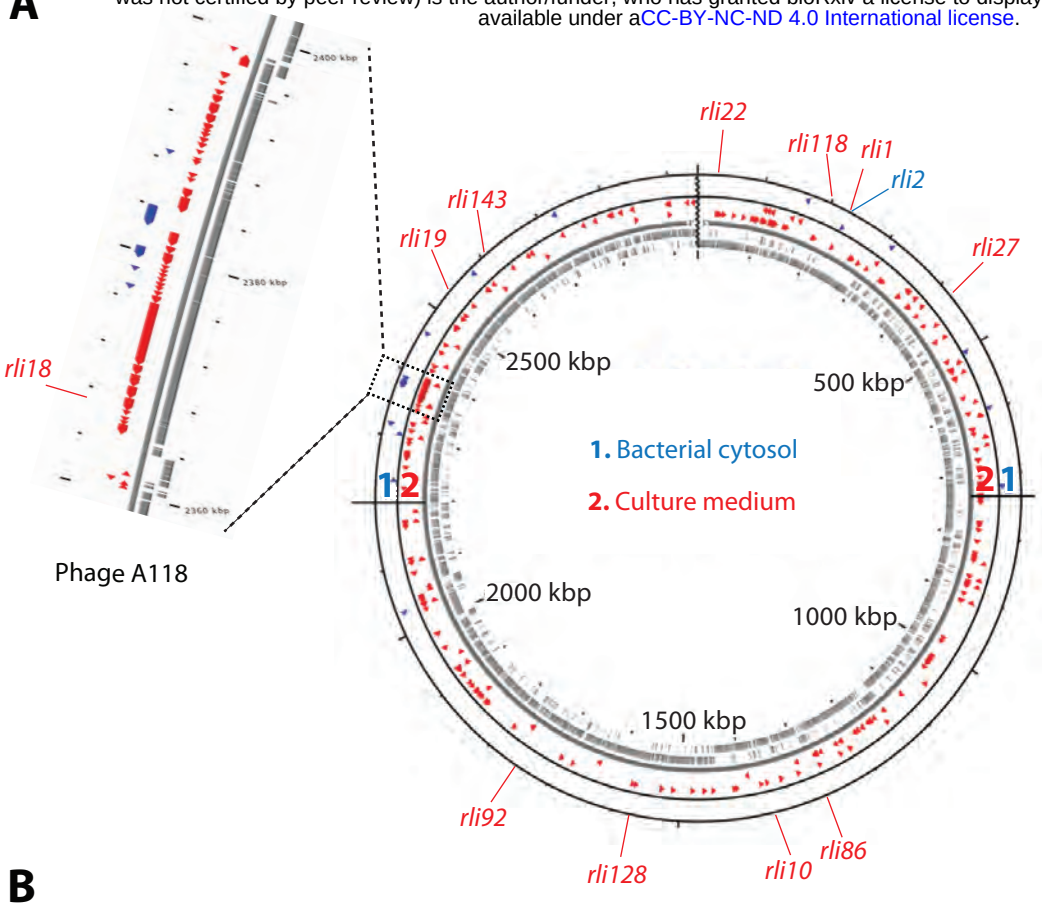

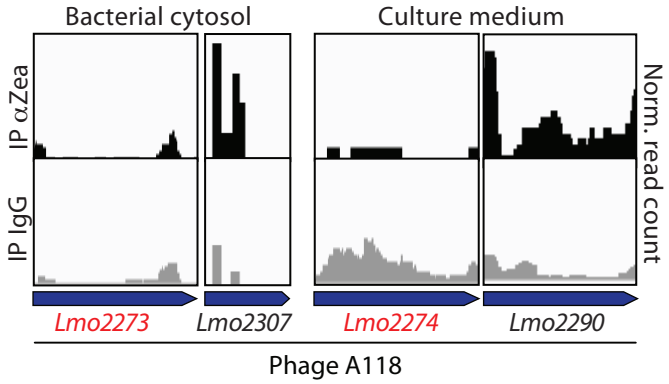

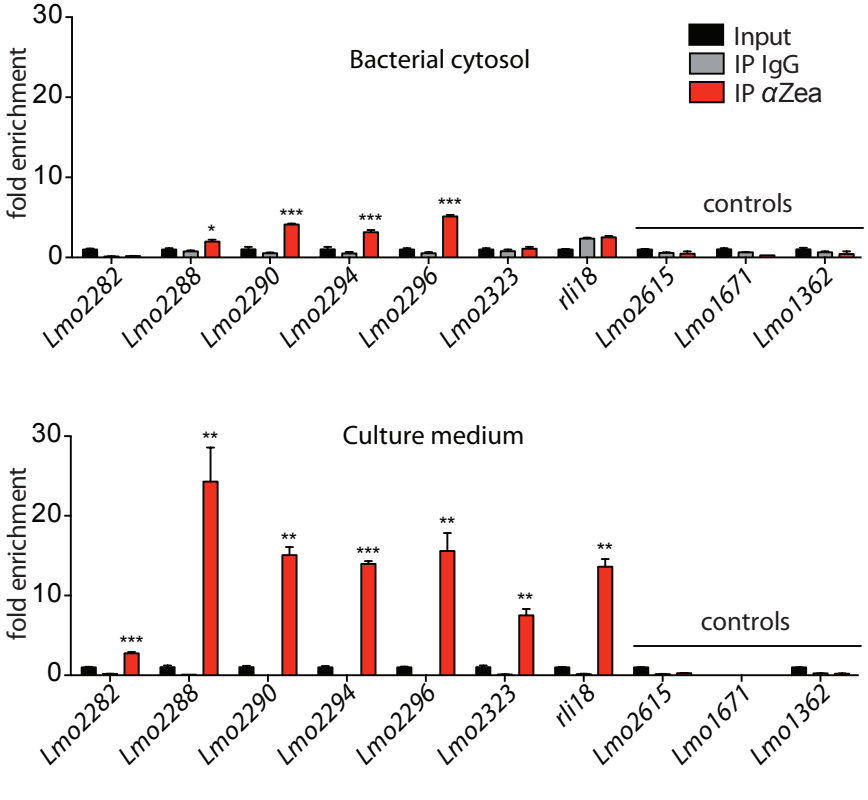

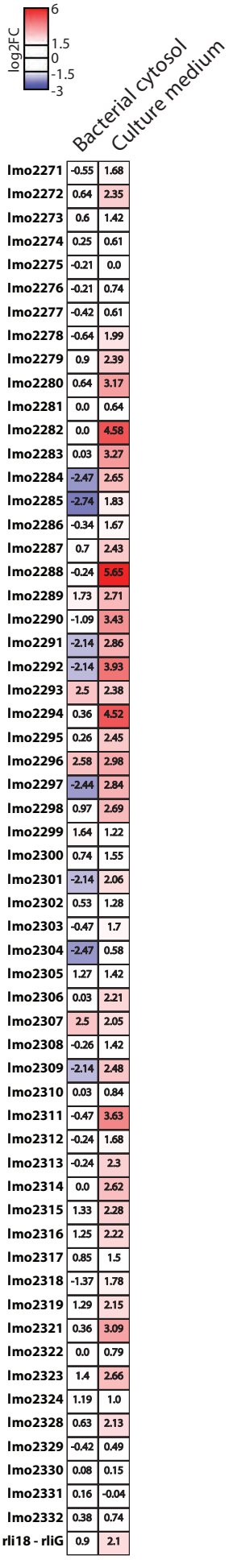

Figure 4

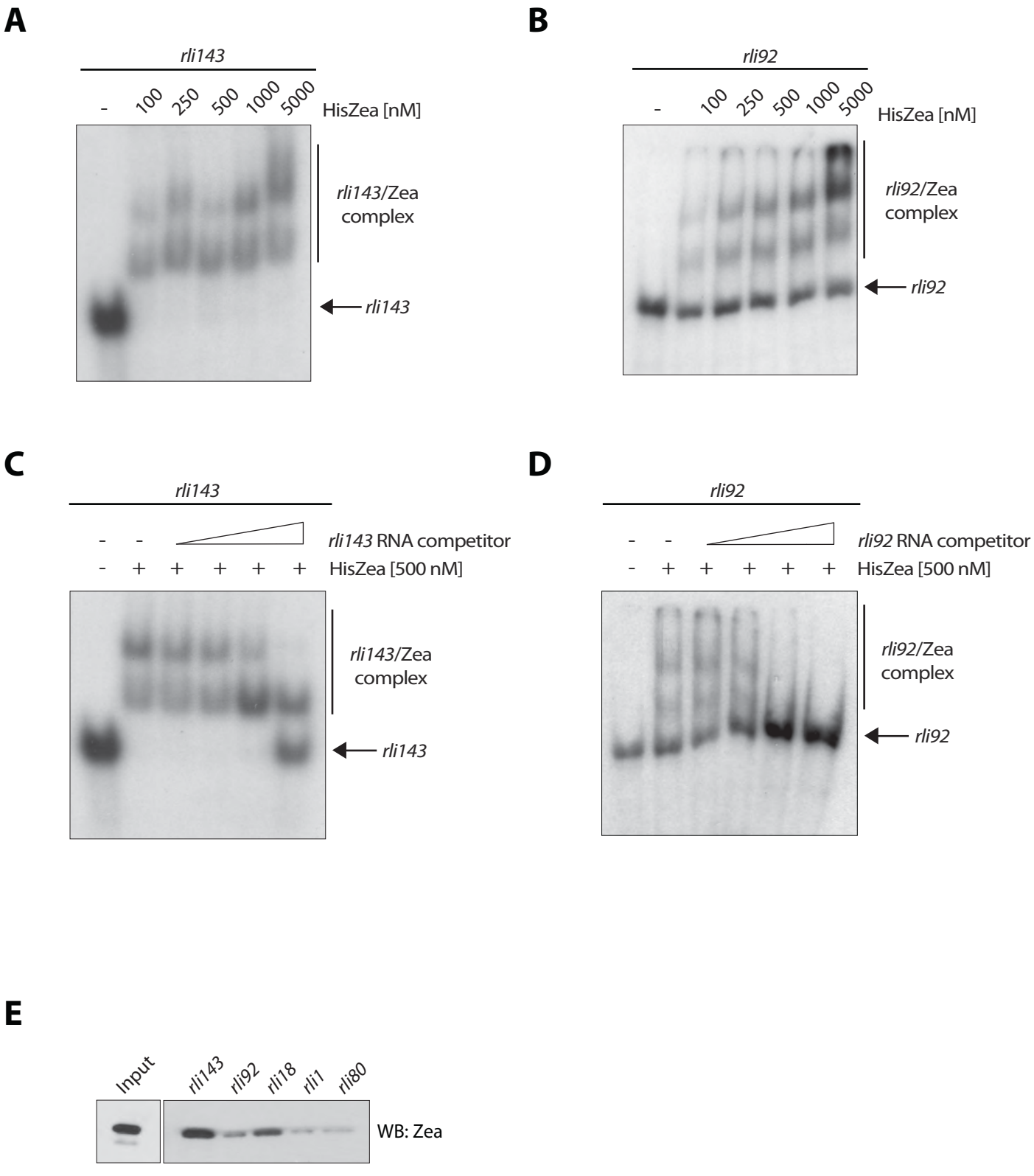

Figure 5

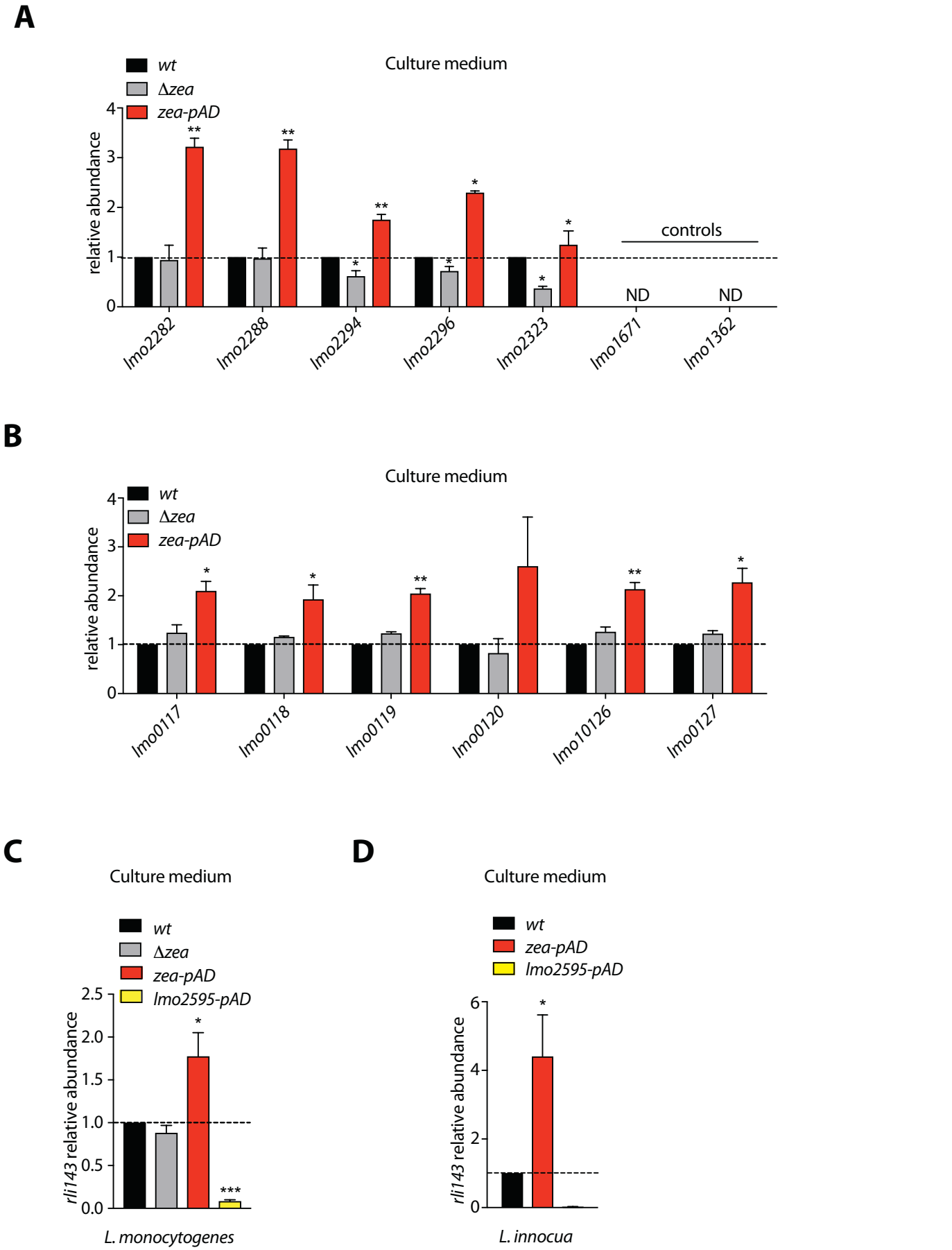

Figure 6

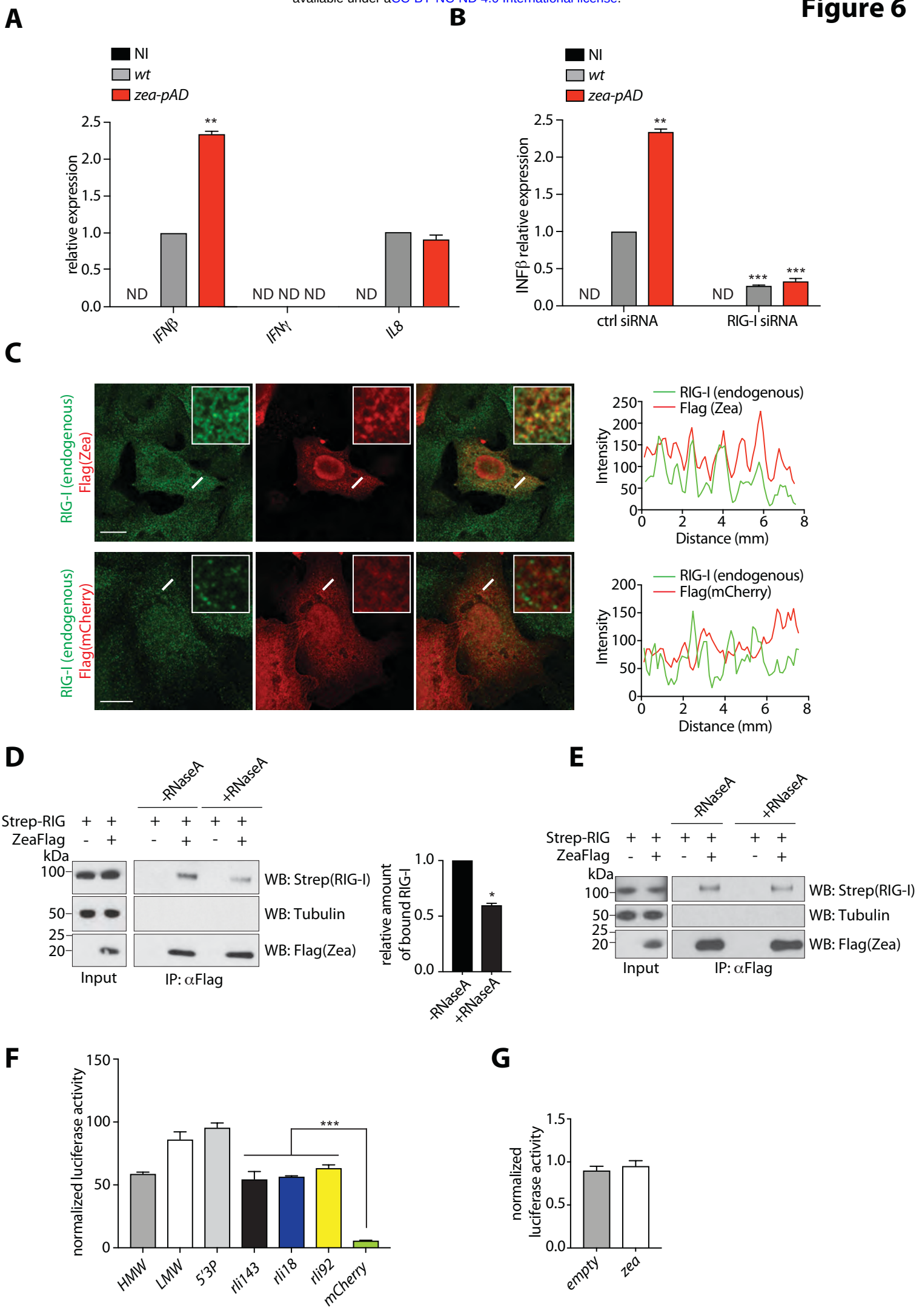

Figure 7